ACS OMEGA

http://pubs.acs.org/journal/acsodf

Article

Novel Thiopyrano[2,3-*d*]thiazole-pyrazole Hybrids as Potential Nonsulfonamide Human Carbonic Anhydrase IX and XII Inhibitors: Design, Synthesis, and Biochemical Studies

Nadia Hanafy Metwally* and Ebrahim Adel El-Desoky

Cite This: *ACS Omega* 2023, 8, 5571−5592

Read Online

ACCESS | Metrics & More | Article Recommendations | Supporting Information

ABSTRACT: In recent years, molecular hybridization strategies have developed into a potent strategy for drug discovery. A series of novel thiopyrano[2,3-*d*]thiazoles linked to the pyrazole moiety was designed and developed as anticancer agents by a molecular hybridization. Target compounds were synthesized and characterized by spectroscopic tools as well as X-ray crystallography analysis as in the case of thiopyrano[2,3-*d*]thiazole derivative **5a**. The MTT assay was used to demonstrate the *in vitro* efficacy of compounds **5a−g** and **7a−j** on MCF-7 and HePG-2. The results showed that some cycloadducts such as bromophenyl-4-thioxo-2-thiazolidinone **3e**, 4-methylphenyl derivative of thiopyrano[2,3-*d*]thiazole **5d**, and 6-substituted-thiopyrano[2,3-*d*]thiazoles **7e−j** displayed good to excellent IC_{50} in the range of 10.08 ± 1.5 to 25.95 ± 2.8 μg/mL against the MCF-7 cell line and from 7.83 ±2.1 to 13.37 ± 1.2 μg/mL against the HePG-2 cell line. To explore the enzymatic tests for isozymes hCAIX and hCAXII, the most promising eight compounds **3e**, **5d**, and **7e−j** with IC_{50} ranging from 7.83 ± 2.1 to 25.95 ± 2.8 μM were chosen. Compound **7e** exhibited an IC_{50} (0.067 ± 0.003 μM) similar to that of the standard drug AZA against CAIX (0.059 ± 0.003 μM)). For CAXII, the compound **7i** had an IC_{50} equal to 0.123 ± 0.007 μM compared to that of AZA (0.083 ± 0.005 μM). In addition, using flow cytometry, cell cycle analysis and apoptosis studies in HePG-2 were performed for the two potent anticancer and selective carbonic anhydrase agents (**7e** and **7i**). An enzymatic assay of these two compounds against caspase-9 was also examined. Interestingly, the molecular docking studies revealed that compounds **7e** and **7i** successfully embedded themselves in the active pockets of the CAIX and CAXII enzymes through different interactions. Overall, the novel thiopyrano[2,3-*d*]thiazole-pyrazole hybrids (**7e** and **7i**) were suggested to be potent and selective inhibitors of CAIX and CAXII.

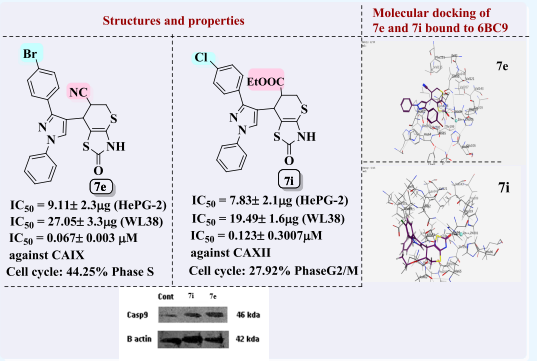

1. INTRODUCTION

Cancer cells have many characteristics that distinguish them from normal cells, such as a more acidic extracellular pH, a slightly alkaline cytoplasmic pH, and a lower than normal oxygen (hypoxia). Hence, the reduced oxygen level, perturbed pH balance, upregulated glucose metabolism, and other aspects of the tumor microenvironment have been viewed as an opportunities to develop antitumor drugs. These drugs specifically target tumor cells without affecting normal cells.[1,2] Studies demonstrated that CA IX and CA XII are biomarkers with therapeutic component for many cancer types.[3−8]

It has been established that carbonic anhydrases (CAs) are crucial for clinical medicine and drug development. Zinc ion, which present in the active site of carbonic anhydrase (CA, EC 4.2.1.1), interacts with water molecules and histidine residues *via* its tetrahedral structure. Through the hydration reaction, the zinc ion binds to the water molecule and catalyzes the transformation of carbon dioxide into bicarbonate ions and protons. This process occurs through a nucleophilic mechanism of metal hydroxide.

CA is crucial to the body's natural defense mechanism.[9−12] Mammals have different 16-CA isozymes, with CA I, CA II, CA III, CA VII, and CA XIII being the first five cytosolic forms. CA IV, CA IX, CA XII, CA XIV, and CA XV are the second five membrane-bound isozymes, along with two mitochondrial forms (CA VA, CA VB), and a secreted CA isozyme (CA VI).[13] The extracellular domain of the transmembrane proteins known as CA IX and CA XII isoform enzymes contains catalytic activity and is important in the control of the tumor microenvironment. Due to its modest expression in normal cells but high expression in solid tumors, CA IX is of particular relevance.[14−16] However, declines in CAIX or CAXII activity seem to have an impact on the pH of

Received: October 28, 2022
Accepted: January 10, 2023
Published: February 6, 2023

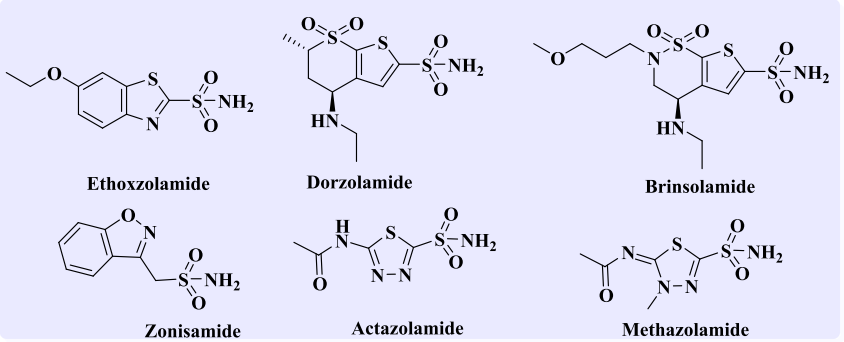

Figure 1. Some known sulfonamide drugs as CA inhibitors.

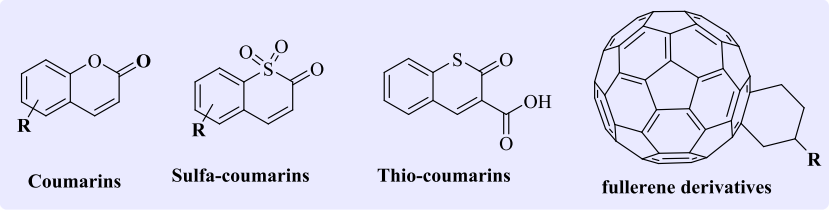

Figure 2. Some nonsulfonamide CA inhibitors.

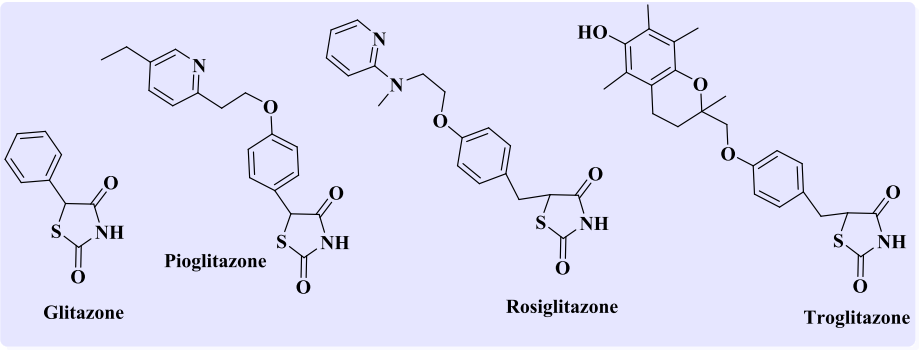

Figure 3. Glitazone derivatives as CAII inhibitors.

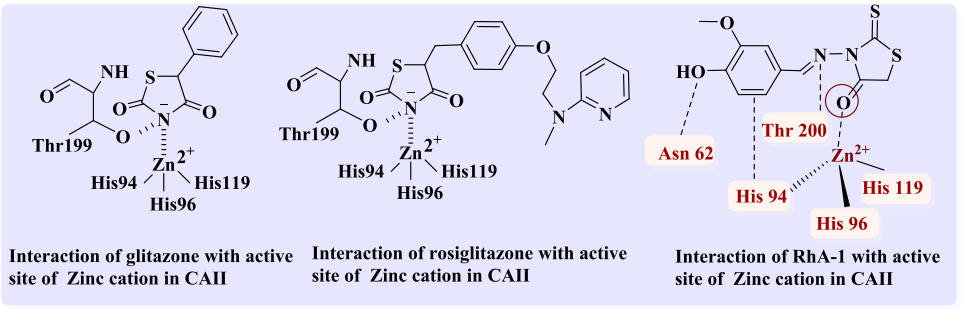

Figure 4. Interaction of glitazone, rosiglitazone, and RhA-1 with the active site of CAII.

the tumor microenvironment, which inhibits the survival and growth of tumor cells.[17,18]

This feature makes CA IX/XII appealing targets for anticancer agents when taken as a whole. This is because of both CAIX and CAXII have well-established roles in the process of tumorigenesis. In preclinical research, a variety of classes of inhibitors and biologics that target CAIX/CAXII have been examined in the processes of cancer signaling, tumor development, acidification, and metastasis. These findings offer encouraging evidence that inhibiting CAIX/CAXII catalytic activity lowers the potential for growth, proliferation, and metastasis of a number of aggressive malignancies both *in vitro* and *in vivo*.[19−22] Classical carbonic anhydrase inhibition occurred by compounds concerning sulfonamide-based (SO_2NH_2) zinc-binding groups (ZBG). These compounds interact with deprotonated catalytic zinc in a tetrahedral shape, which inhibits CA activity by displacing the water/hydroxide ions bound to the zinc (Figure 1). Some sulfonamide drugs are currently being used clinical setting as CA inhibitors, although

https://doi.org/10.1021/acsomega.2c06954
ACS Omega 2023, 8, 5571−5592

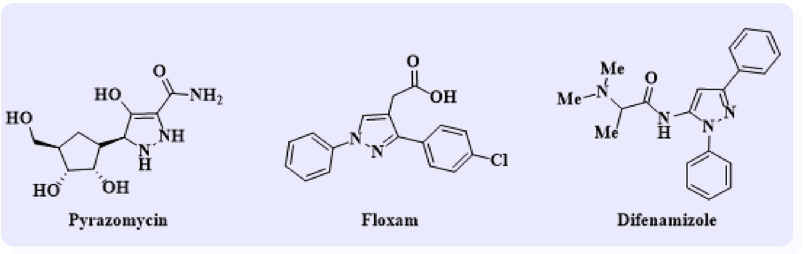

Figure 5. Marked drugs of pyrazole derivatives.

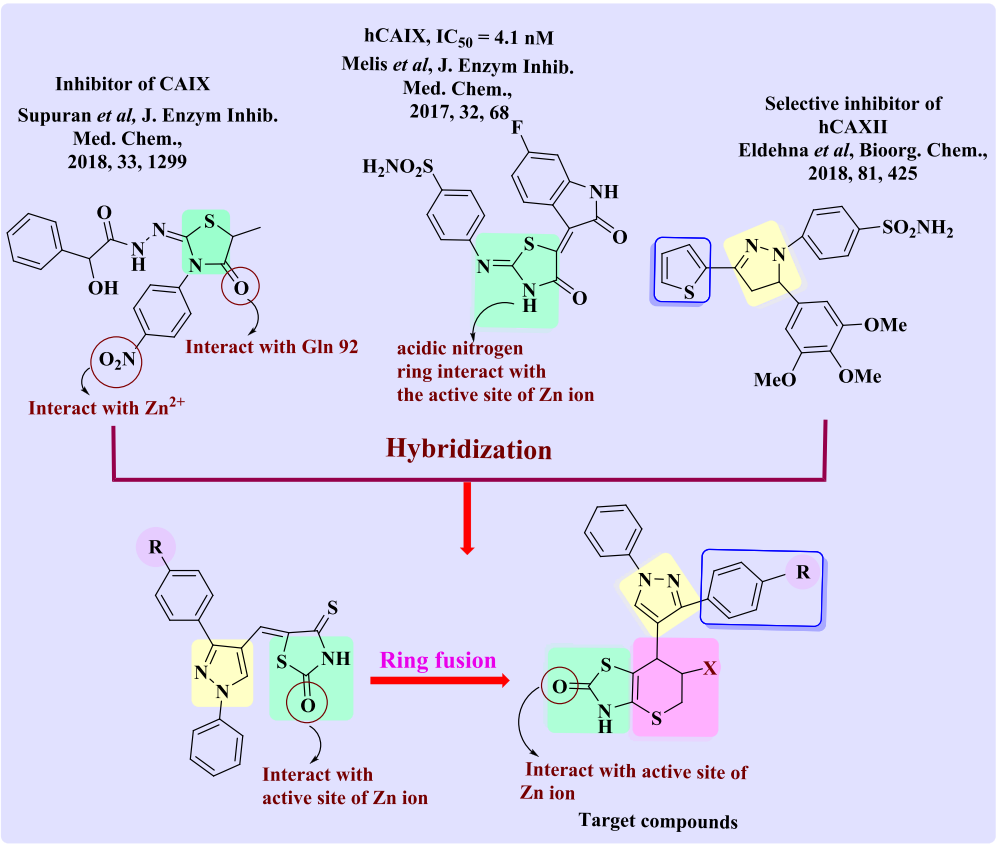

Figure 6. Design strategy for the synthesis of thiopyrano[2.3-*d*]thiazoles (color codes indicate general chemical structures).

3 to 6% of the general population are allergic to them because of untreatable sulfur allergies.

Moreover, nonsulfonamide CA inhibitors like phenols, polyamines, carboxylic acids, coumarins, thiocoumarins, and their derivatives exhibit a binding mechanism that is a typical of conventional sulfonamide CA inhibitors, as they are anchored to zinc-bound water/hydroxide ions or bind outside the active site to inhibit substrate entry (Figure 2). Many hCAIX inhibitors of such concept had synthesized, including aromatic sulfonamides, open saccharins and isatin derivatives. For example, currently, in clinical trials, 4-[(4-fluorophenyl)-carbamoyl]aminobenzene sulfonamide (SLC-0111) seems to be a potent CA inhibitor.[23−25] It is also conceivable for other inhibitor binding mechanisms to attach to the allosteric or activating region without interacting directly with zinc ions.

Important heterocyclic rings with many beneficial biological properties include thiazolidinone core, which have anti-inflammatory, antibacterial, antifungal, antiviral, anticancer, anticonvulsant, and antitubercular properties.[26−28] Furthermore, glitazone and their analogues were also recognized as CAII inhibitors such as nonsulfonamide 5-phenyl-2,4-thiazolidinedione (Figure 3). The findings suggested a connection between the zinc cation at the active site and the acidic nitrogen ring (Figure 4).[29] In addition, other glitazone derivatives like pioglitazone, rosiglitazone, and troglitazone demonstrated considerable binding and inhibition of the CAII isozyme through interaction between the acidic imide NH and the active site zinc.[30] As an example, the interaction between rosiglitazone and active site of CAII has an ionic bond of 2.0 Å between the imide nitrogen and the active site Zn cation and only one hydrogen bond between the imide and Thr199 of 3.1 Å.

Other 4-thiazolidinones interact with the zinc active site through a carbonyl group on a ring that is not the acidic imide NH ring. As an illustration, 3-[(4-hydroxy-3-methoxybenzylidene)amino]-2-thioxothiazolidin-4-one (RhA-1) forms hydrogen bonds with Asn 62 and Thr 200, and the benzyl ring forms an aromatic hydrogen bond with His 94. The 2-thioxothiazolidine scaffold that formed an aromatic bond interacted with Zn 265 of hCA II (Figure 4).[31] Hence,

https://doi.org/10.1021/acsomega.2c06954
ACS Omega 2023, 8, 5571−5592

Scheme 1. Synthesis of 5-[(3-Aryl-1-phenyl-1*H*-pyrazol-4-yl)methylene]-4-thioxo-2-thiazolidinones 3a−e

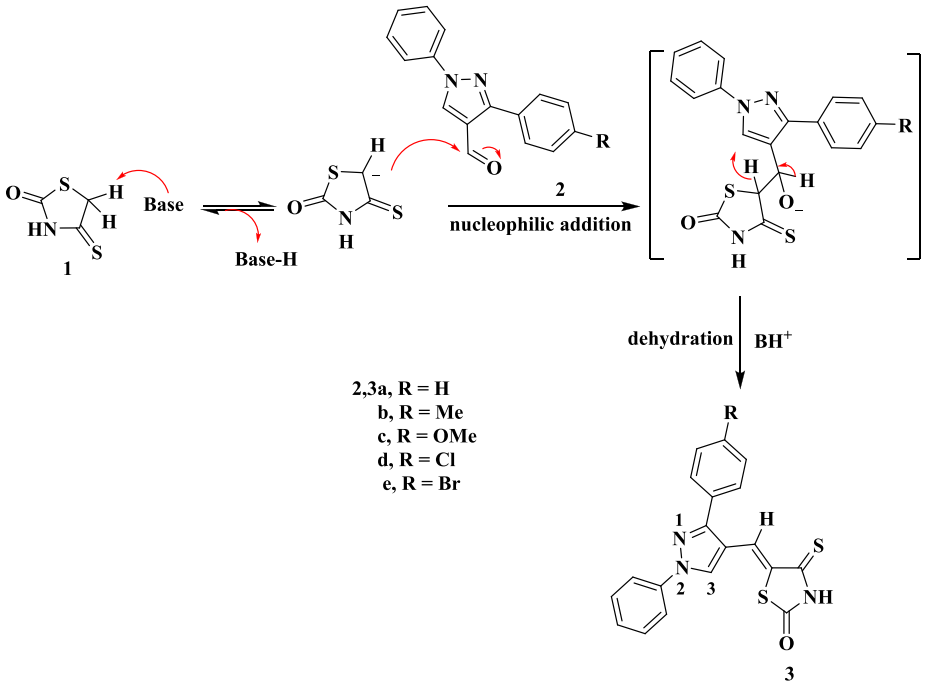

Scheme 2. Synthesis of 8-(3-Aryl-1-phenyl-1*H*-pyrazol-4-yl)-6-arylpyrrolo[3′,4′:5,6]thiopyrano[2,3-*d*]thiazole-2,5,7-triones 5a−g

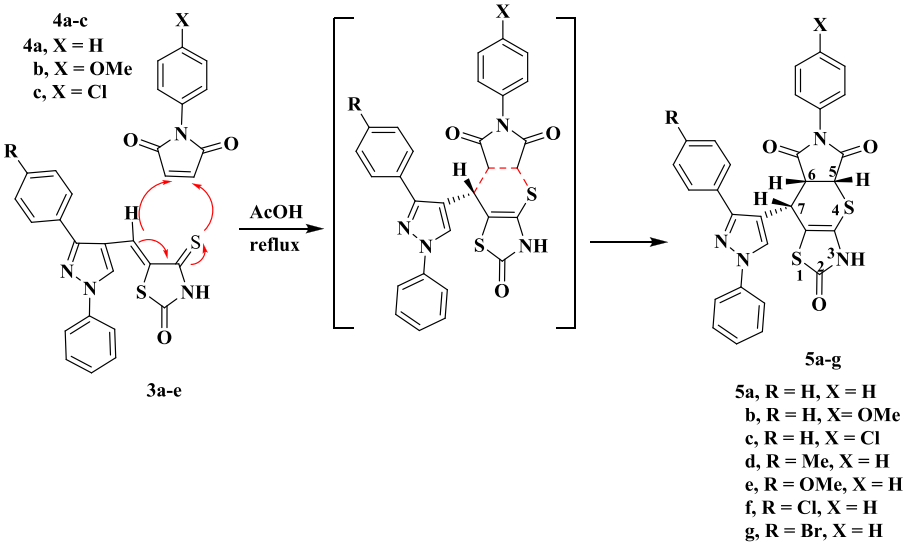

thiazolidinedione derivatives may represent exciting opportunities for the development of novel CA inhibitors as future drugs (Figure 4).

The molecular hybridization strategy is a novel approach to develop hybrid multifunctional molecules by combining two or more pharmacophores in a single scaffold. Another instance is the formation of the innovative anti-tuberculosis (TB) chemotype benzo[*d*]thiazol-2-yl(piperazin-1-yl)-meth-anone through hybridization of the piperazine moiety with benzo-[*d*]thiazole-2-carboxamide.[32] Furthermore, hybridization of ethyl 1-phenyl-1*H*-benzo[*d*]imidazole-2-carboxylate with alicyclic amines yielded benzo[*d*]imidazole-2-carboxamides as anti-TB agents[33] and others.[34−37] The presence of two or more biologically active pharmacophores within a single unit not only synergizes the biological activity but also enhances the ability to interact with more than one biological target.[38] Moreover, the pyrazole ring system also has a wide range of biological activities, including antifungal,[39] antimicrobial,[40] anticancer,[41−43] anti-AIDS,[44] and antidepressants.[45] The pyrazole ring system is an important bioactive ingredient in over-the-counter drugs such as pyrazomycin (anticancer drug), floxan (anti-inflammatory drug), and difenamizole (non-steroidal anti-inflammatory drug) (Figure 5).

Considering the foregoing and continuing to synthesize diverse ring systems with potential biological applications,[46−58] molecular hybridization approaches were applied to synthesize two series of compounds by combining the above nuclei. The first series contained of pyrazoles connected to thiopyrano[2,3-*d*]thiazole hybrids (**5a−g**) *via* *N*-aryl maleimides with **3a−d**, and the second series consisted of pyrazole-linked thiopyrano-

https://doi.org/10.1021/acsomega.2c06954
ACS Omega 2023, 8, 5571−5592

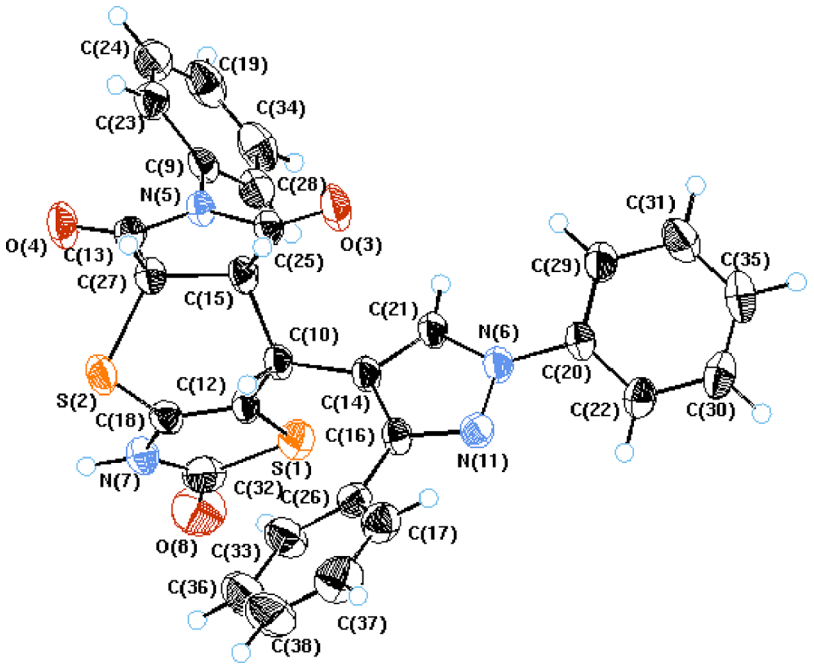

Figure 7. X-ray crystallography of cycloadduct **5a.**

[2,3-*d*]thiazoles hybrid (**7a−j**) with a cyano or ester group (Figure 6).

2. RESULTS AND DISCUSSION

2.1. Chemistry. A *Knoevenagel* condensation was carried out between 4-thioxo-2-thiazolidinone **1** and 1-phenyl-3-aryl-1*H*-pyrazole-4-carbaldehydes **2a−e**, providing 5-pyrazolyl-methylene-4-thioxo-2-thiazolidinones **3a−e** according to Scheme 1. The chemical structures of **3a−e** were proven by spectroscopic tools. As an example, compound **3a** revealed two singlet signals at δ 8.70 and 13.75 ppm representing the pyrazole-H-5 and NH protons, respectively, along with an aryl multiplet in the range of δ 7.29 to 8.0 ppm in the ^{1}H NMR chart. ^{13}C NMR revealed significant signals at δ 153.12, 170.25, and 194.79 ppm corresponding to pyrazole-C-3, carbonyl, and thiocarbonyl carbons, respectively, and along with it are signals corresponding to aromatic carbons, thiazolidine-C-5 and vinyl-C. The IR spectrum of **3a** showed characteristic absorption bands at 3434 and 1736 cm^{-1} due to the NH and C═O groups, respectively. Mass spectrometry showed an ion peak at m/z = 363 (M^+). The proposed mechanism is that a base deprotonates the alpha-carbon of 4-thioxo-2-thiazolidinone **1**, to give an anion. This anion attacks the carbonyl function in aldehydes **2** to produce an aldol-like intermediate, which undergoes dehydration to produce the final products as shown in Scheme 1.[59]

Additionally, compounds **3a−e** were reacted with *N*-aryl maleimides **4a−c** in refluxing acetic acid to yield 1:1 adducts **5a−g** (Scheme 2). The assigned structures for the products **5a−g** were established on spectroscopic tools. In compound **5e**, the IR spectrum represent absorption bands at 3445, 1716 and 1674 cm^{-1} corresponding to N−H and two C═O groups, respectively. The ^{1}H NMR chart contains a singlet at δ 3.81 ppm to the OCH_3 group, a doublet of doublets at δ 4.20 ppm with *J* values of 3.0 and 9.0 Hz corresponding to H-6, a doublet at δ 4.92 ppm with a *J* value of 3.0 Hz due to H-5, and a doublet signal at δ 4.94 ppm with a *J* value of 9.0 Hz attributed to H-7 in addition to the multiplet at δ 7.07−7.96 ppm corresponding to the aryl protons and two singlets at δ 8.56 and 11.75 ppm attributed to pyrazole-H-5 and NH protons, respectively. Its mass spectrum exhibited, among other the fragments, ion peaks at m/z = 566 (M^+). The formation of compounds **5a−g** proceeds *via* a concerted mechanism based on the hetero-Diels−Alder reaction, using compounds **3a−g** as heterodienes and *N*-aryl maleimides **4a−c** as dienophiles, as shown in Scheme 2.[60]

Derived from proton nuclear magnetic resonance data, **5a−g** have only one stereoisomer, (*Z*-isomer) arising from the deshielding of vinyl proton, which is effected by the C═S moiety of the thiazole ring, leading to a lower magnetic field ($\delta \approx$ 7.88−7.94 ppm) than the *E*-isomer appearing at higher magnetic fields ($\delta \approx$ 7.30−7.60 ppm).[61] This consumption was also proven by X-ray crystallographic analysis of compound **5a**. We noticed from determination of X-ray data that the most important aspect of this structure is the relative stereochemistry of the H atoms at the stereoisomeric C-25, C-27, and C-10 centers. The C-25 and C-27 hydrogen atoms have a *cis*-axial−axial orientation, while the C-10 hydrogen atom occupies an axial position relative to the dihydrothiopyran ring (Figure 7).

Under the same reaction conditions, **3a−e** reacted with dienophiles **6a,b** to yield the 1:1 cycloadducts, which was formulated as 7-(3-aryl-1-phenyl-1*H*-pyrazol-4-yl)-2-oxo-3,5,6,7-tetrahydro-2*H*-thiopyrano[2,3-*d*]thiazole derivatives **7a−j** (Scheme 3). From the spectral data, structures **7a−j** were assigned to these adducts, so the **7d**'s IR spectrum showed absorption bands at 3442, 2245, and 1644 cm^{-1} corresponding to the N−H, CN, and CO groups, respectively. The ^{1}H NMR chart appeared a multiplet signal at δ 3.44−3.64 ppm assigned to H-5, a multiplet signal at δ 3.99 ppm to H-6, and a doublet signal at δ 4.53 ppm with a *J* value of 5.1 Hz to H-7. Also clarified were multiplet signals ranging from δ 7.33−7.92 ppm assigned to aryl protons and two singlets at δ 8.61 and 11.49 ppm corresponding to pyrazole-H-5 and NH protons (D_2O exchangeable), respectively. The ^{13}C NMR

https://doi.org/10.1021/acsomega.2c06954
ACS Omega 2023, 8, 5571−5592

Scheme 3. Synthetic Route of 7-(3-Aryl-1-phenyl-1*H*-pyrazol-4-yl)-2-oxo-3,5,6,7-tetrahydro-2*H*-thiopyrano[2,3-*d*]thiazole Derivatives 7a−j

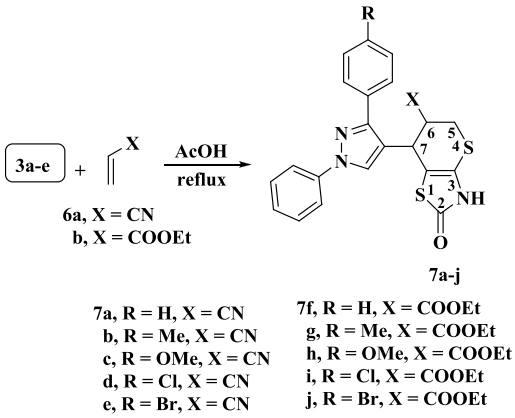

spectrum observed significant signals at 27.03, 31.54, and 33.13 ppm for C-5, C-7, and C-6, respectively. Mass spectrometry showed ion peaks at m/z = 452 (M^++2), 451 (M^++1), and 450 (M^+), consistent with the molecular formula $C_{22}H_{15}ClN_4OS_2$.

3. BIOLOGICAL ACTIVITY

3.1. Anticancer Activity. The cytotoxicity of the tested compounds **3a−e**, **5a**, **5d−g**, and **7a−j** assessed human breast cancer (MCF-7) and hepatocellular carcinoma (HePG-2) by the MTT assay and utilizing doxorubicin as a standard drug. The data on *in vitro* cytotoxicity were expressed as IC_{50}, which is the compound concentration (in μg/mL) that decreased cell viability by 50% (Tables 1−3 and Figures 8−10). The MCF-7

Table 1. IC_{50} Values of Compounds 3a−e against MCF-7 and HePG-2 Cell Lines

compound no.	R	IC_{50} in μg/mL MCF-7	IC_{50} in μg/mL HePG-2
doxorubicin		4.17 ± 0.2	5.57 ± 0.4
3a	H	52.11 ± 3.1	65.75 ± 3.3
3b	Me	56.27 ± 3.4	62.16 ± 3.2
3c	OMe	37.59 ± 3.4	31.22 ± 2.6
3d	Cl	30.84 ± 2.2	38.20 ± 2.7
3e	Br	11.16 ± 1.5	10.66 ± 1.0

Table 2. IC_{50} Values of Compounds 5a and 5d−g against MCF-7 and HePG-2 Cell Lines

compound no.	R	X	IC_{50} in μg/mL MCF-7	IC_{50} in μg/mL HePG-2
doxorubicin			4.17 ± 0.2	5.57 ± 0.4
5a	H	H	30.30 ± 0.4	38.42 ± 2.1
5d	Me	H	25.95 ± 2.8	21.31 ± 1.8
5e	OMe	H	35.72 ± 72	30.70 ± 0.3
5f	Cl	H	25.40 ± 2.1	29.0 ± 2.1
5g	Br	H	42.91 ± 2.7	44.96 ± 3.0

and HePG-2 cell lines were shown to be sensitive to the tested compounds based on how the synthetic compounds affected the proliferation of the two cancer cell lines.

Preliminary *in vitro* anticancer screening results indicate that most of the compounds tested exhibited IC_{50} ranging from 10.08 ± 1.5 to 67.32 ± 3.7 μg/mL against the MCF-7 cell line. In the first series of **3a−e**, compounds **3a** and **3b** showed weak activity against the two cell lines tested, while compounds **3c**

Table 3. IC_{50} Values of Compounds 7a−j against MCF-7 and HePG-2 Cell Lines

compound no.	R	X	IC_{50} in μg/mL MCF-7	IC_{50} in μg/mL HePG-2
doxorubicin			4.17 ± 0.2	5.57 ± 0.4
7a	H	CN	23.76 ± 1.9	26.84 ± 3.3
7b	Me	CN	35.03 ± 2.3	30.42 ± 1.1
7c	OMe	CN	29.43 ± 1.1	24.12 ± 2.9
7d	Cl	CN	67.32 ± 3.7	73.05 ± 4.3
7e	Br	CN	10.10 ± 2.1	9.11 ± 3.2
7f	H	COOEt	15.90 ± 2.3	13.37 ± 1.2
7g	Me	COOEt	12.30 ± 2.4	11.87 ± 2.7
7h	OMe	COOEt	11.36 ± 1.5	12.18 ± 1.1
7i	Cl	COOEt	10.08 ± 1.5	7.83 ± 2.1
7j	Br	COOEt	11.80 ± 4.0	10.26 ± 4.8

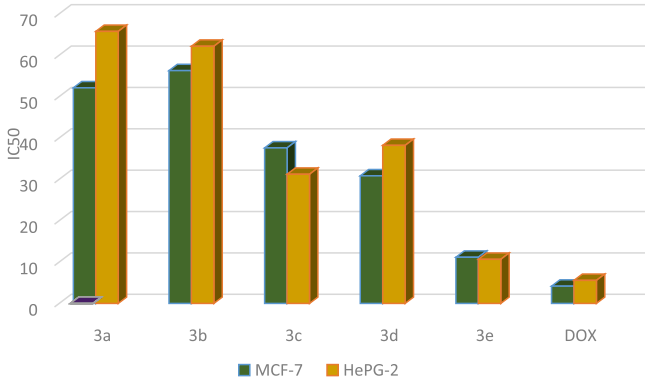

Figure 8. Graph representing the IC_{50} values of compounds **3a−e** against MCF-7 and HePG-2 cell lines, indicating that **3e** is the most potent cytotoxic agent in this series using doxorubicin as standard drug.

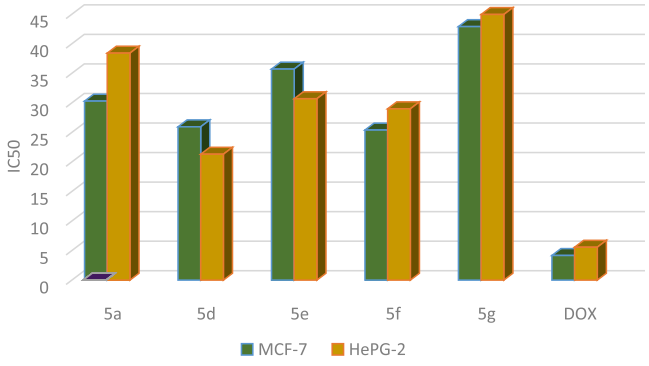

Figure 9. Graph showing the IC_{50} values of compounds **5a** and **5d−g** against MCF-7 and HePG-2 cell lines, indicating that **5d** in this series has a good cytotoxic effect using the MTT colorimetric method and doxorubicin as a reference.

and **3d** showed moderate activity. Moreover, compound **3e** exhibits a strong anticancer activity against MCF-7 cell line with IC_{50} = 11.16 ± 1.5 μg/mL. On the other hand, the sensitivity of compounds **3a−e** to the HePG-2 cell line showed an IC_{50} ranged from 7.83 ± 1.5 to 73.05 ± 4.3 μg/mL. Compound **3e** showed strong cytotoxic activity with IC_{50} = 7.83 ± 1.5 μg/mL among the other prepared series **3a−e** (Table 1 and Figure 8). In a second series of thiopyrano[2,3-*d*]thiazoles **5a−g**, the most active compound **5d** exhibited IC_{50} = 25.40 ± 2.1 and 21.31 ± 1.8 μg/mL, against MCF-7 and HePG-2 cells, respectively, while compound **5g** was weakly

https://doi.org/10.1021/acsomega.2c06954
ACS Omega 2023, 8, 5571−5592

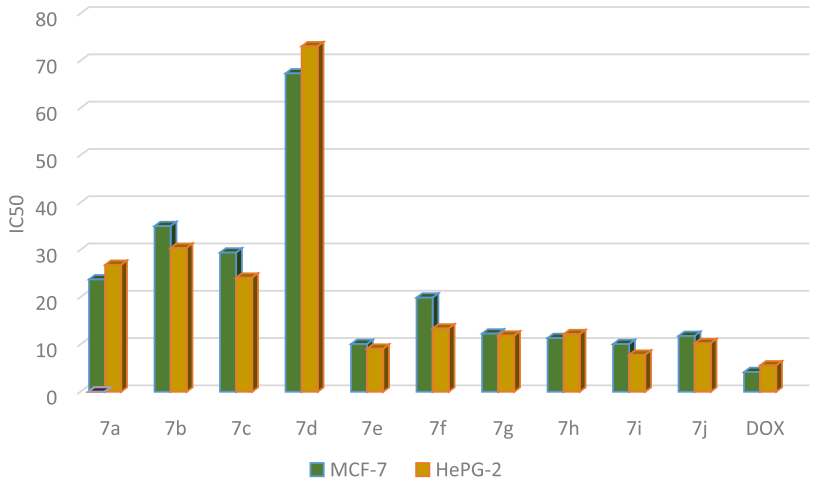

Figure 10. Graph representing the IC_{50} values of compounds **7a–j** against MC-7 and HePG-2 cell lines, indicating that compounds **7e–j** have good anticancer activity against MCF-7 and HePG-2.

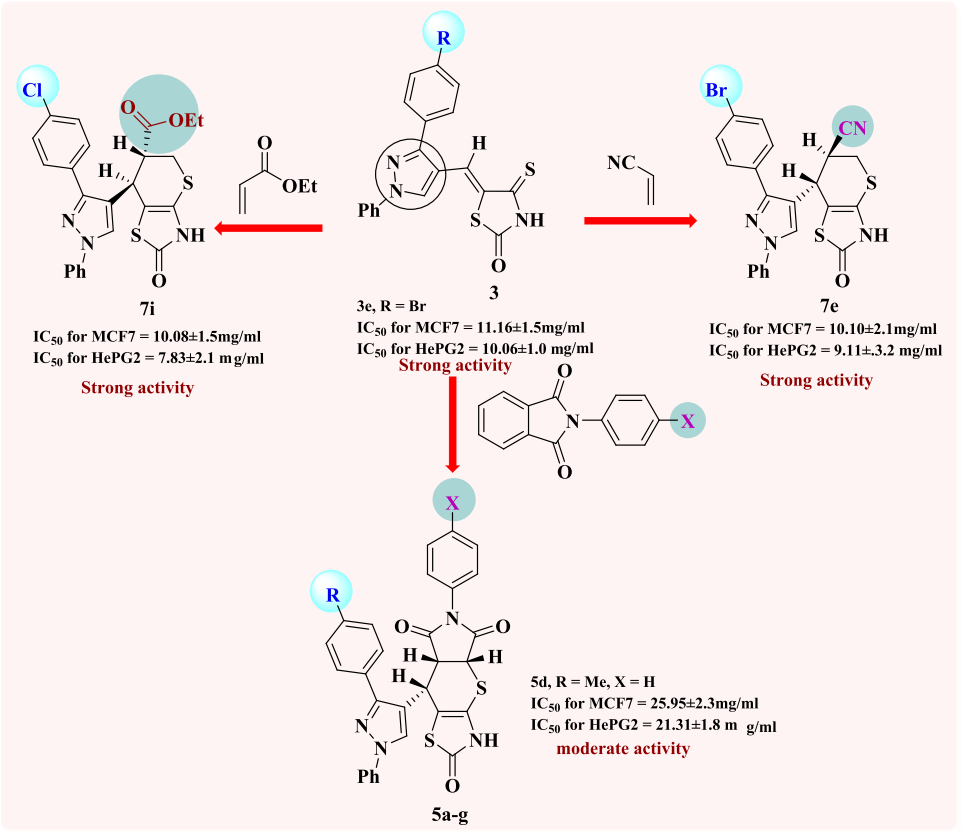

Figure 11. Structure–activity relationship (SAR) of the targets **3**, **5a–g**, **7e**, and **7i**.

active toward the two cell lines in this series (Table 2 and Figure 9). The last series, cycloadducts **7a–j** revealed moderate to strong anticancer activity against MCF-7 and HePG-2 cell lines. Thus, **7e** and **7i** were the most potent anticancer activity of all the tested compounds in this series, with IC_{50} = 10.10 ± 2.1 and 10.08 ± 1.5 μg/mL, respectively, for MCF-7, while HePG-2 have IC_{50} = 9.11 ± 3.2 and 7.83 ± 2.1 μg/mL, respectively. Other compounds **7g**, **7h**, and **7j** appeared strong cytotoxicity against MCF-7 and HePG-2, while compounds **7a–c** and **7f** showed moderate anticancer activity, whereas compound **7d** showed weak activity as shown in Table 3 and Figure 10

3.2. Structure–Activity Relationship (SAR). Based on the data revealed, it is possible to conclude structure–activity relationships for the synthesized target compounds, as shown in Figure 11.

(1) As demonstrated in Figure 11, the substituents on the benzene ring and thiopyrano moiety have a significant impact on the activity and broadness, which can be summed up as follows.

(2) The presence of a bromine atom on a phenyl ring incorporated to a pyrazole moiety (electron-withdrawing group, −ve inductive effect) in the starting **3a–e** is required

https://doi.org/10.1021/acsomega.2c06954
ACS Omega 2023, 8, 5571−5592

to show the broad spectrum cytotoxic activity against MCF-7 and HePG-2, which represents **3e**.

(3) On the other hand, the presence of a methyl group in the phenyl ring linked to the pyrazole moiety reduces the activity against MC-F7 and HePG-2 as in **3b**.

(4) In series a of cycloadducts **5a** and **5d−g**, introduction of a bromine atom into the phenyl ring of the pyrazole moiety reduced activity against MCF-7 and HePG-2 as in **5g**.

(5) The results from the previous part of this series show that the presence of an electron donating group, such as a methoxy group, enhanced the cytotoxic activity toward the two cell lines (compound **5e**).

(6) Compound **5f** showed almost moderate activity against MCF-7 and HePG-2 due to the presence of a chlorine atom as an electron withdrawing group.

(7) The results for the final cycloadducts **7a−j** show that the presence of an electron withdrawing group (Br) at the 4-position of the phenyl ring of the pyrazole moiety increases the negative inductive effect on the reactive center of the molecule, resulting in increased cytotoxic activity for compounds **7e**, **7i**, and **7j**, expect compound **7d**.

(8) Compounds with a methyl or methoxy group as a donor group at the 4-position of the phenyl ring and cyano group as an electron-withdrawing group at the thiopyran moiety showed moderate cytotoxicity activity (compounds **7b** and **7c**).

(9) Compounds with a methyl or methoxy group at the 4-position of the phenyl ring and an ester group on the thiopyran moiety showed the similar effects and increased the cytotoxic activity (compounds **7g** and **7h**).

(10) Compounds **5a**, **7a**, and **7f**, with no substituents on the phenyl ring, showed moderate cytotoxic activity. Therefore, compounds **3e**, **5d**, and **7e−j** were chosen for enzyme inhibition investigation.

3.3. *In Vitro* Cellular Viability. Data obtained from cell viability in WI38 (human lung fibroblast cell line) are listed in Table 4 and Figure 12 for compounds **3a−e**, **5a**, **5d−g**, and **7a−j**. The results reveal that compounds **3a**, **3b**, and **5g** with moderate anticancer activity in the MCF-7 and HePG-2 revealed strong cell viability at IC_{50} = 28.20 ± 2.3, 25.27 ± 2.1, and 24.86 ± 2.0 μg, respectively, on WI38. Compounds **7e**, **7h**, and **7i**, with strong anticancer activity with IC_{50} = 27.05 ± 3.3, 25.34 ± 2.2, and 19.49 ± 1.6 μg, respectively, show high cell survival values at WL38.

Table 4. IC_{50} of the Target Compounds against Human Lung Fibroblast Cell Line WI38

compound no.	IC_{50} in μg/mL WI38
DOX	8.87 ± 0.6
3a	28.20 ± 2.3
3b	25.27 ± 2.1
3c	64.53 ± 3.8
3d	71.21 ± 4.2
3e	41.48 ± 2.9
5a	65.68 ± 1.1
5d	49.86 ± 3.4
5e	51.67 ± 3.7
5f	43.02 ± 3.1
5g	24.86 ± 2.0
7a	54.64 ± 3.5
7b	41.35 ± 1.7
7c	51.91 ± 3.4
7d	39.49 ± 1.7
7e	27.05 ± 3.3
7f	44.50 ± 4.5
7g	30.31 ± 1.7
7h	25.34 ± 2.2
7i	19.49 ± 1.6
7j	33.76 ± 2.5

3.4. Enzyme Inhibition. *3.4.1. In Vitro hCA-IX and hCA-XII Inhibition.* The most potent anticancer compounds **3e**, **5d**, **7e**, and **7e−j** were evaluated for their potential as inhibitors of human carbonic anhydrase IX and XII isoforms using acetazolamide (AZA) as a standard. All the tested compounds significantly inhibited CAIX activity, with IC_{50} values ranging from 0.067 ± 0.003 to 0.928 ± 0.045 μM. As demonstrated in Table 5 and Figure 13, the IC_{50} values for CAXII ranged from 0.123 ± 0.007 to 1.047 ± 0.057 μM.

Data listed in Table 5 showed that compound **7e** was more potent (IC_{50} = 0.067 ± 0.003 μM) against the CAIX isoform like AZA (IC_{50} = 0.059 ± 0.003 μM). Compound **7h** has lower activity against hCAIX than that of compound **7e**, with an IC_{50} value of 0.133 ± 0.006. Compounds **3e**, **5d**, and **7g** showed nearly identical IC_{50} values 0.349 ± 0.011, 0.336 ± 0.016, and 0.390 ± 0.019 μM, respectively. Compounds **7i** and **7j** also have IC_{50} in the same range equal to 0.287 ± 0.014 and 0.239 ± 0.03 μM, respectively. Compound **7f** was found to be the weakest active hit in the series with an IC_{50} = 0.928 ± 0.045 μM (Table 5 and Figure 13). In the CAXII assay studies, compound **7i** was the most potent hCAXII inhibitor in the series, with IC_{50} = 0.123 ± 0.007 μM, compared to the standard drug. Compound **7e** was found to have a lower IC_{50} than **7i** (0.202 ± 0.011 μM). On the other hand, compounds **3e**, **5d**, **7g**, **7h**, and **7j** have nearly identical activity against CAXII, with IC_{50} values of 0.556 ± 0.016, 0.604 ± 0.033, 0.566 ± 0.031, 0.049 ± 0.022 and 0.589 ± 0.03 μM, respectively, but compound **7f** still showed the weakest activity against CAXII with an IC_{50} = 1.047 ± 0.057 μM, compared to the other compounds tested in this series as shown in Table 5 and Figure 13. Thus, it is noteworthy that compounds **7e** (contains 4-bromo) and **7i** (containing 4-Cl atom) showed excellent inhibition against CAIX and CAXII isoforms because of their electron-withdrawing groups. Compound **7e** was a more potent and selective CAIX inhibitor than the other prepared series and compatible with the standard drug AZA, while compound **7i** was potent and selective to CAXII inhibitor and its IC_{50} is close to AZA. Based on the above information, compounds **7e** and **7i** were selected for further biological investigation.

3.4.2. Cell Apoptosis and Necrosis. Based on the data obtained from the cytotoxic activity and carbonic anhydrase inhibitory effect, compounds **7e** and **7i** appear to be the most potent and selective cytotoxic effect agents in the HePG-2 cell line, exhibiting significant inhibitory potency against the two carbonic anhydrases, CAIX and CAXII. To demonstrate the mechanistic effects on the cell cycle of compounds **7e** and **7i** (at concentrations of IC_{50} values), with the lowest IC_{50} values in the HePG-2 cell line, we selected them for further investigation. Flow cytometry was performed on MCF-7 cell lines using propidium iodide (PI) and annexin V-FITC to determine the cell number at each mitosis. After treatment of thiopyrano[2,3-*d*]thiazoles **7e** and **7i** with HePG-2 for 24 h, the corresponding red (PI) and green (FITC) fluorescence was detected by flow cytometry. It was found that treatment of HePG-2 cells with cycloadducts **7e** and **7i** significantly

https://doi.org/10.1021/acsomega.2c06954
ACS Omega 2023, 8, 5571−5592

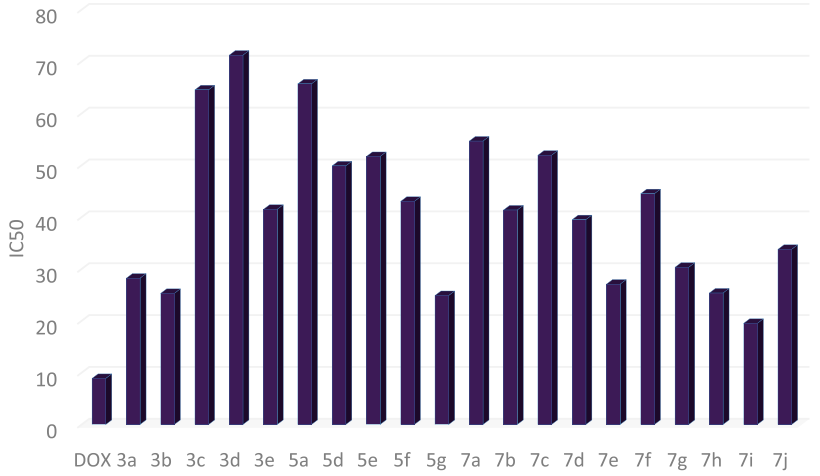

Figure 12. Cell viability in the human lung fibroblast cell line WI38 for all synthetic compounds.

Table 5. Carbonic Anhydrase Inhibition Data of the Tested Compounds 3e, 5d, 7e−i, and Standard Drug AZA

compound	CAIX IC_{50} (μM)	CA XII IC_{50} (μM)
3e	0.349 ± 0.011	0.556 ± 0.016
5d	0.336 ± 0.016	0.604 ± 0.033
7e	0.067 ± 0.003	0.202 ± 0.011
7f	0.928 ± 0.045	1.047 ± 0.057
7g	0.390 ± 0.019	0.566 ± 0.031
7h	0.133 ± 0.006	0.409 ± 0.022
7i	0.287 ± 0.014	0.123 ± 0.007
7j	0.239 ± 0.03	0.589 ± 0.03
AZA	0.059 ± 0.003	0.083 ± 0.005

increased the percentage of annexin V-FITC-positive apoptotic cells, containing the early from 0.55 to 11.91 (lower right cytogram quadrant) for compound **7e** and from 0.55 to 28.71 for compound **7i** compared to control. However, in the late apoptosis, the results showed that the proportion of annexin V-FITC-positive apoptotic cells for compound **7e** was 21.24 (upper right cytogram quadrant). Late apoptosis of compound **7i** is 9.51. In conclusion, compounds **7e** and **7i** increase the early apoptotic ratios by 21-fold and 52-fold compared to control cells, whereas the late apoptotic % increases approximately 101-fold and 45-fold, respectively. Moreover, compounds **7e** and **7i** exhibited nearly the same necrosis results of 3-fold compared to the control cell HePG-2 (1.39). These results indicated that compound **7i**, which was investigated, had an apoptosis inducing effect on HepG-2 cells at an early stage, while compound **7e** had a stronger apoptotic inducing effect at a late stage, and both compounds **7e** and **7i** induced the apoptosis rather than the necrotic pathway through the programmed cell death pathways (Table 6 and Figures 14−17).

Table 6. Cell Content % in Initial and Late Apoptosis on HePG-2 Cells Treated with Compounds 7e and 7i besides the Percent of Necrosis

	apoptosis			
compound	total	early	late	necrosis
7e/HePG2	36.28	11.91	21.24	3.13
7i/HePG2	41.13	28.71	9.51	2.91
Cont.HePG2	2.15	0.55	0.21	1.39

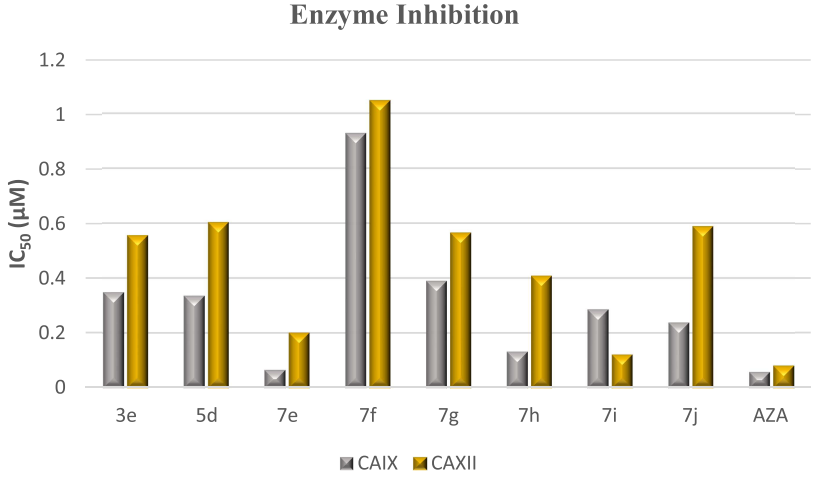

Figure 13. Graph comparing the carbonic anhydrase inhibition data for the target compounds **3e**, **5d**, and **7e−j** with the standard drug acetazolamide (AZA), showing that compound **7e** is a potent and selective CAIX inhibitor and compound **7i** is a potent and selective CAXII inhibitor compared to the reference drug.

https://doi.org/10.1021/acsomega.2c06954
ACS Omega 2023, 8, 5571−5592

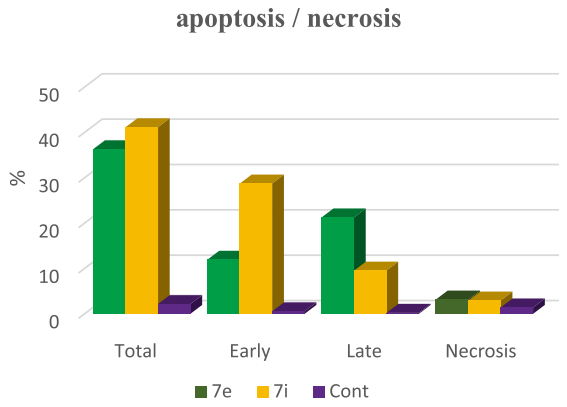

Figure 14. Chart showing the percent of cells in apoptosis and necrosis on HePG-2 cells treated with **7e** and **7i.**

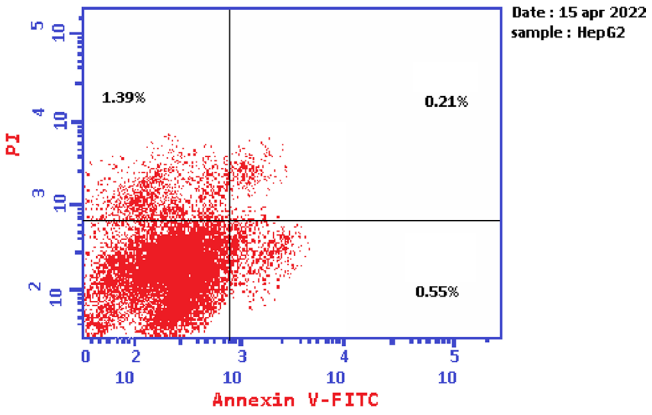

Figure 15. Graph showing the cell population in apoptosis and necrosis in HePG-2.

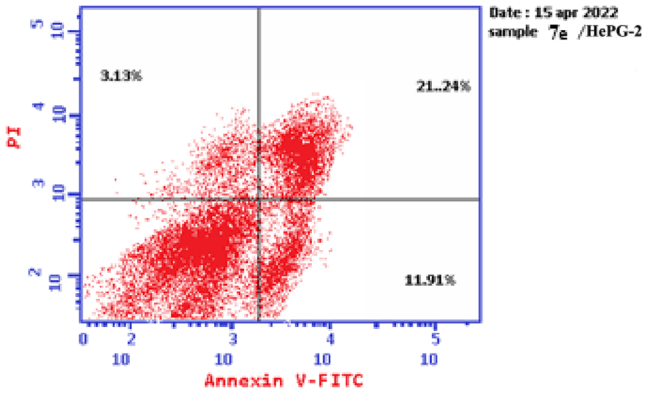

Figure 16. Graph representing the cell apoptosis and necrosis in HePG-2 cells treated with **7e.**

3.4.3. Cell Cycle Detection. The effects of thiopyrano[2,3-*d*]thiazoles **7e** and **7i** on cell cycle progression were performed on HePG-2 cancer cell lines, through a DNA flow cytometry. HePG-2 cells were treated with cycloadducts **7e** and **7i** at IC_{50} concentrations (9.11 and 7.83, respectively) for 24 h. The results of this assay demonstrated that exposure of HePG-2 cells to compounds **7e** and **7i** led to the percentage of cells in the S phase and G2/M was significantly increased by **7e** and **7i**. Compared to the control, compound **7e** increased the cell ratio by 1.2-fold in phase S, while compound **7i** increased the cell ratio by 1.6-fold in phase G2/M. HepG-2 cells. Thus, the HepG2 was arrested in phase S in the cell cycle by compound

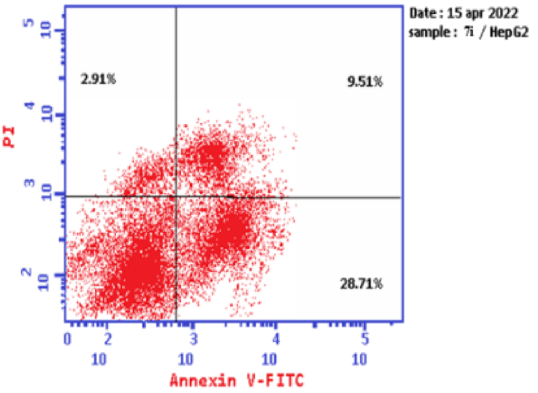

Figure 17. Graph showing the cell apoptosis and necrosis in HePG-2 cells treated with **7i.**

7e, whereas cells were arrested in phase G2/M by compound **7i** (Table 7 and Figures 18−21). Therefore, compounds **7e** and **7i** bind to the molecules involved in S and G2/M phases, respectively.

Table 7. Cell Cycle Analysis of Compounds 7e and 7i

code	%G0−G1	%S	%G2/M	comment
7e/HePG2	41.39	44.25	14.36	cell growth arrest@S
7i/HePG2	39.56	32.51	27.93	cell growth arrest@G2/M
Cont.HePG2	46.32	35.99	17.69	

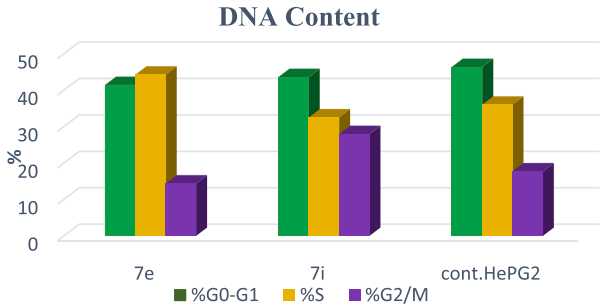

Figure 18. Cell cycle graph of the most potent compounds **7e** and **7i.**

3.4.4. Cell Cycle Analysis. **3.5. Caspase 9 Assay.** Apoptosis is a tightly controlled form of cell death that gets rid of unhealthy or dysfunctional cells. A range of internal or environmental factors can cause apoptosis. One of two signaling routes can be activated by a stimulus, depending on its source (internal or external). Both processes require caspases, which can be divided into initiator caspases and effector caspases. Caspases are aspartate-specific cysteine proteases. Caspases play a vital role in initiating the apoptotic process. Caspase activation ensures a controlled method of degradation of cellular components with minimal impact on surrounding tissue. Caspase-9 is a key initiator caspase in the apoptotic pathway and is activated during endogenous trigger apoptosis.[62] When HePG-2 cells were treated with **7e** and **7i**, an increase in caspase-9 concentration was observed, as shown in Table 8. Compared to control, compound **7e** showed a significant increase (almost 4-fold) in the level of active caspase-9. Compound **7i** also showed significant increase by 3-fold compared to the control as shown in Table 8 and Figures 22 and 23.

https://doi.org/10.1021/acsomega.2c06954
ACS Omega 2023, 8, 5571−5592

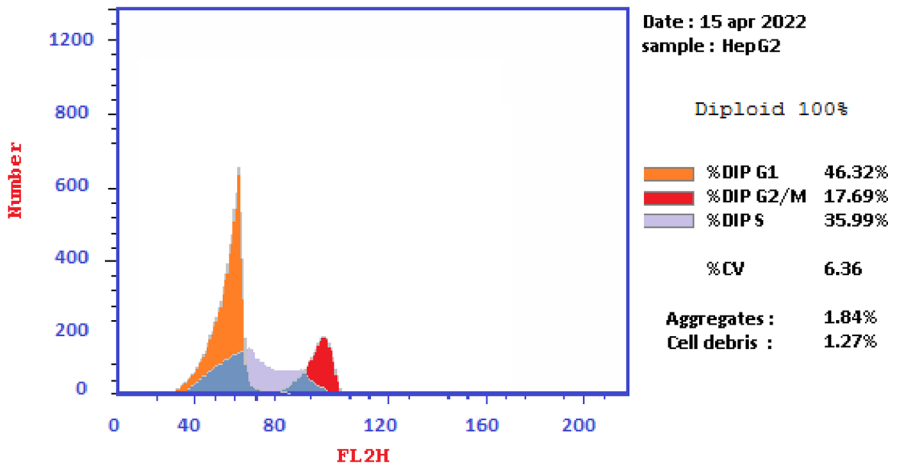

Figure 19. Graph showing the DNA content % in the HePG-2.

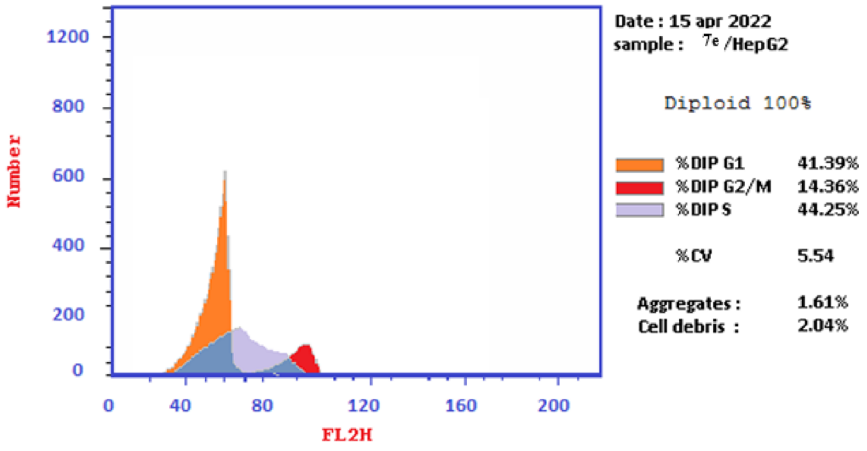

Figure 20. Graph showing the DNA content % in the HePG-2 treated with **7e** *via* division phases expressing the arrest of cell cycle in the S phase.

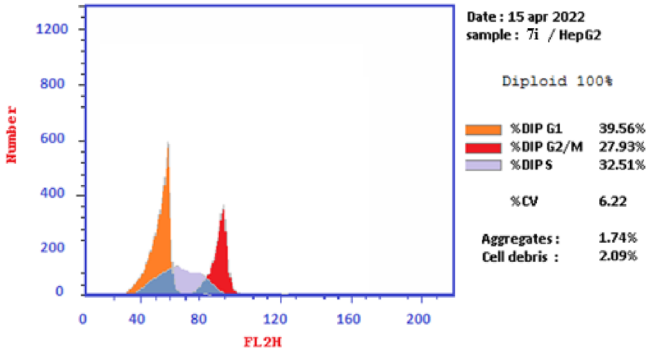

Figure 21. Graph showing the DNA content % in the HePG-2 treated with **7i** *via* division phases expressing the arrest of the cell cycle in the G2/M phase.

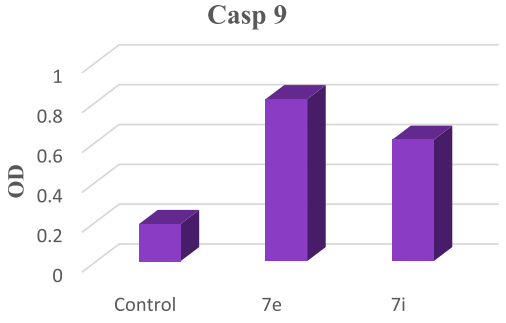

Figure 22. Impact of **7e** and **7i** on caspase 9, indicating that compounds **7e** and **7i** have an effect on it.

Table 8. Results of Caspase 9

	Casp9	
compound	OD	*β*-actine
7e/HepG2	0.813	+
7i/HepG2	0.609	+
Cont.HepG2	0.186	+

Image J analysis was also performed to estimate the protein levels in caspase-9, as shown in Figure 26. Analysis revealed that the level in caspase cells, treated with compound **7i**, was 2.98-fold compared to the untreated cell, whereas compound **7e** resulted in greater levels of caspase-9 than in untreated cells by 7.143-fold (the values calculated after normalization to *β*-actin). These results are consistent with those obtained from measuring caspase 9 activity utilizing Western Blot assay.

3.6. Molecular Docking Study. Molecular Operating Environment (MOE 2015. 10) software was used to explore the potential binding modes for the most active compounds, **7e**, **7i**, and **7h**, as well as their isomers, with the active sites of CAIX and CAXII [(*R*)-5-(2,4-dimethoxybenzyl)-2-thioxothiazolidin-4-one)] (5U0F in PDB) in order to explain the

https://doi.org/10.1021/acsomega.2c06954
ACS Omega 2023, 8, 5571−5592

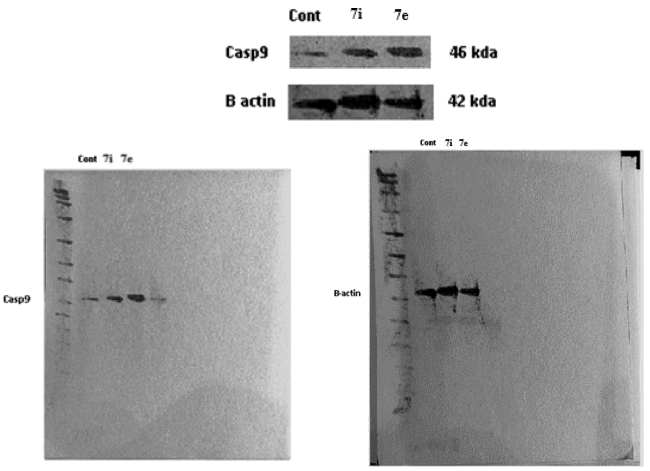

Figure 23. Effect of the targets **7e** and **7i** on Caspase 9 using Western Blot method.

observed carbonic anhydrase inhibitory activity and to understand the potential mechanism (Figure 24).

The standard drug AZA binds to the active site and provides four interactions. This included the interaction of one hydrogen bond of the sulfoxide function group (S═O) with Thr A199 with a bond length of 2.79 Å, and the ionic interaction of the zinc ion (Zn 301) with another sulfoxide group. The binding energy of interactions is −2.2591 kcal/mol and rmsd-fine 1.4460 as depicted in Table 9 and Figure 25. The most active **7e**, which is found in the two isomers **7ea** and **7eb**, presented the interactions for adopted by the co-crystallized ligand binding to the active site amino acids including His A94, which interacts with the phenyl group in the thiazole ring by an arene-H bond as well as an ionic bond between the carbonyl of the thiazole and zinc ion 301 for **7ea** (Figure 26), whereas the second isomer, **7eb**, exhibited an ionic interaction between Zn 301 and the cyano group, in addition to the interaction between the sulfur atom of the thiazole ring and Thr 200 with a bond length of 3.75 Å (Figure 26). The interaction binding energy of isomer **7ea** (−2.2591 kcal/mol) is smaller than that of **7eb** (−4.6934 K cal/mol), so the isomer **7ea** is favored in the interaction. Compound **7i** is also found in two isomers, **7ia** and **7ib**. Isomer **7ia** binds to the active pocket of 5U0F by zinc ion 301 with a thiazole ring carbonyl group (Figure 27). On the other hand, carbonyl group of **7ib**, with rmsd_refine 0.9538 at S = −5.6139 binds to Asn 62 together with arene-H with Leu 128 (Figure 27). The isomer **7ia** is therefore more acceptable due to the ionic

Table 9. Interactions of Compounds 7e, 7i, 7h, and AZA with 5U0F

compound no.	energy S kcal/mol	rmsd−refine	amino acids contributed in the interaction	length of bonds Å
AZA	−2.2591	1.4460	Thr 199	H-bond 2.97 Å (S═O)
			Zn 301	ionic bond (S═O)
7ea	−6.5441	1.3601	His 94	arene-H of phenyl ring
			Zn 301	C═O thiazole ring
7eb	−4.6934	0.9475	Zn 301	CN group
			Thr 200	arene-H of S-thiazole
7ia	−6.7493	2.0325	Zn 301	C═O of thiazole ring
7ib	−5.6139	0.9538	Asn 62	C═O thiazole ring
			Leu 128	arene-H of phenyl ring
7ha	−6.9086	1.8485	Zn 301	C═O of thiazole ring
7hb	−6.1544	1.7606	His 64	C═O of thiazole ring

interaction of the Zn ion. Similarly, compound **7h** also interacts with the pock of the active site of 5U0F by an ionic bond with zinc ion 301 as demonstrated in Figure 28 for **7ha**, whereas **7hb** has one interaction between the carbonyl group and His 64 of S = −5.1544 kcal/mol (Figure 28). From the interaction patterns of compounds **7e**, **7i**, and **7h**, we concluded that the presence of the carbonyl group on thiazole ring is important for the interaction with the active site pocket of 5U0F (see table 3).

4. CONCLUSIONS

A new class of thiopyrano[2,3-*d*]thiazoles were synthesized and assessed for their anticancer activity. Cycloadducts **7e** and **7i** displayed potent anticancer activity at low concentrations. The antiproliferative activity of cycloadducts **7e** and **7i** appeared to correlate well with their ability to inhibit both CAXI and CAXII isoforms at submicromolar levels. Cycloadduct **7e** is emerged as the most potent hCAIX inhibitor with an IC_{50} value of 0.067 ± 0.003 μM, while compound **7i** is also a more potent and selective CAXII inhibitor (IC_{50} = 0.123 ± 0.007 μM) compared to the standard drug acetazolamide AZA. Therefore, we screened cycloadducts **7e** and **7i** for cell cycle disruption of HePG-2 and found that the % of annexinV-FITC positive apoptotic cells increased from 11.91 to 21.24% for

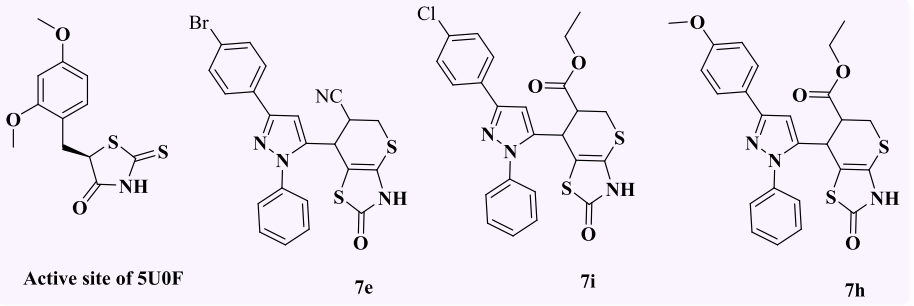

Figure 24. The most active compounds **7e**, **7i**, and **7h** against CAIX and CAXII with (*R*)-5-(2,4-dimethoxybenzyl)-2-thioxothiazolidin-4-one) [PDB code: 5U0F].

https://doi.org/10.1021/acsomega.2c06954
ACS Omega 2023, 8, 5571−5592

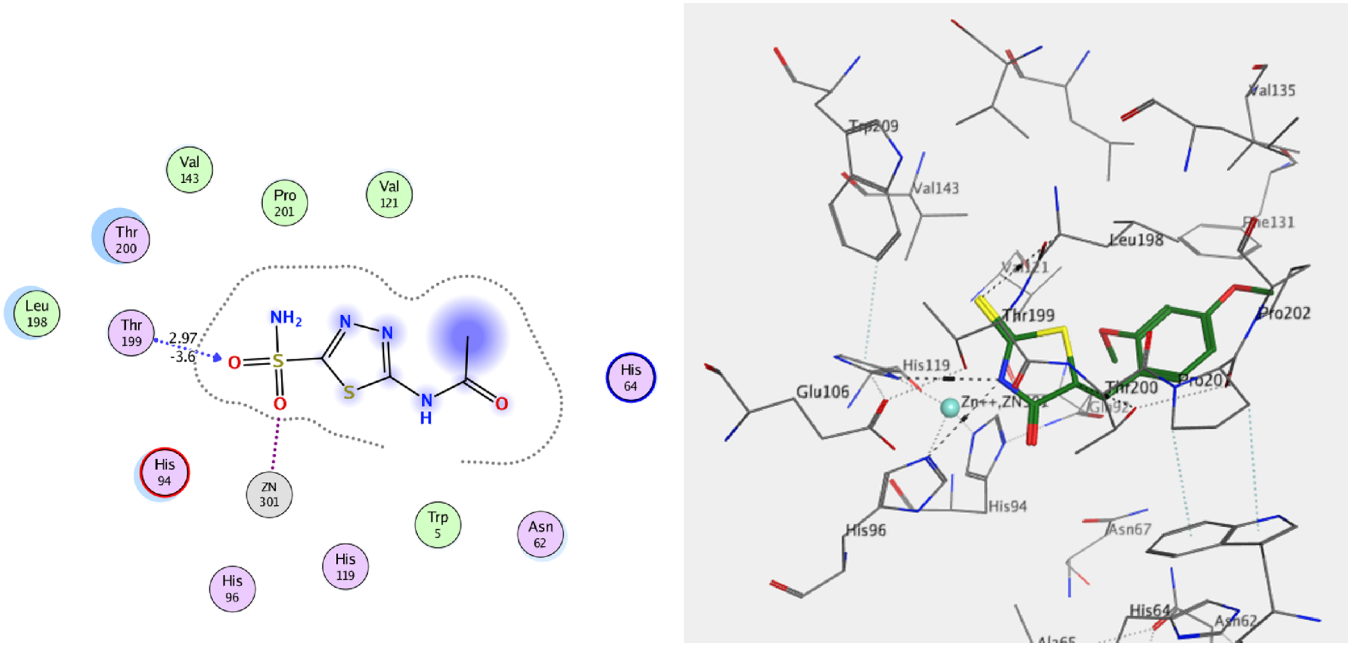

Figure 25. 2D and 3D of **AZA** with an active pocket of 5U0F.

compound **7e** and decreased from 28.71 to 9.51% for compound **7i** in cells. This investigated the mechanistic pathways of compounds **7e** and **7i** in cells and confirmed that they significantly increased the levels of active caspase-9. Finally, to rationalize the obtained results, we performed molecular docking studies of thiopyranothiazoles **7e** and **7i** within CAIX and XII active sites (PDB; 5U0F). Thiopyrano-[2,3-*d*]thiazoles **7e** and **7i** are privileged multitargeted scaffolds for the development of novel anticancer drugs as well as CAIX and CAXII inhibitors.

5. EXPERIMENTAL SECTION

5.1. Chemistry. The uncorrected melting points for all materials were calculated using an Electrothermal (9100) device, and the IR spectra were captured using KBr pellets on a Perkin Elmer 1430 spectrophotometer. The NMR spectra were recorded on a Varian Mercury VXR-300 NMR spectrometer and recorded at 300 and 75 MHz (^{1}H and ^{13}C NMR spectra, respectively) using DMSO-d_6 as solvent, with results are expressed as δ values. A Shimadzu GCMS-QP 1000 Ex mass spectrometer was used to measure the mass spectra at a voltage 70 eV. At Cairo University's Microanalyses Center, an elemental analysis was carried out using a Vario EL III Elemental CHNS analyzer. The University of Zürich's Institute of Organic Chemistry conducted the X-ray crystallographic analysis. The pharmacy faculty at Egypt's Mansoura University engaged in anticancer activity. At VACSERA (holding company for biological products and vaccines Cairo, Egypt), the enzyme inhibition, cell cycle, apoptosis, and caspase-9 were measured. Beginning materials **1**, **2a−e**, and **4a−c** were acquired using the procedures previously described.[63−65]

*5.1.1. Synthesis of 5-[(3-Aryl-1-phenyl-1H-pyrazol-4-yl)-methylene]-4-thioxo-2-thiazolidinone Derivatives **3a−e**.* **5.2. General Procedure.** 3-Aryl-1-phenyl-1*H*-pyrazole-4-carbaldehydes **2a−e**, 4-thioxo-2-thiazolidinone **1**, and fused sodium acetate were all refluxed in 20 mL of glacial acetic acid for 2 h before being left to stand at room temperature overnight. The precipitate that resulted was filtered, washed with water, dried, and then recrystallized from the mixture of ethanol and dioxane.

*5.2.1. 5-[(1,3-Diphenyl-1H-pyrazol-4-yl)methylene]-4-thioxo-2-thiazolidinone (**3a**).* Red crystals; 56%; mp 271 °C; IR (KBr, cm^{-1}) 3434 (NH), 1736 (CO); ^{1}H NMR (DMSO-d_6): δ = 7.29−8.0 (m, 11H, 10 Ar-H and olefinic-H), 8.70 (s, 1H, pyrazole-H), 13.75 (s, 1H, NH, D_2O exchangeable); ^{13}C NMR (DMSO-d_6): δ = 116.40, 119.41, 125.70, 127.55, 127.98, 128.42, 129.50, 129.62, 130.34, 133.98, 138.50, 139.16, 153.12, 170.25, 194.79; *m*/*z* (%) = 364 (6.6, M$^+$+1), 363 (22.1, M$^+$), 286 (4.6), 232 (5.7), 209 (1.7), 144 (3.7), 77 (100.0). Anal. calcd for $C_{19}H_{13}N_3OS_2$ (363.46): C, 62.79; H, 3.61; N, 11.56; S, 17.64. Found: C, 62.52; H, 3.88; N, 11.74; S, 17.41%.

*5.2.2. 5-[(3-(4-Methylphenyl)-1-phenyl-1H-pyrazol-4-yl)-methylene]-4-thioxo-2-thiazolidinone (**3b**).* Orange crystals; 40%; mp 293 °C; IR (KBr, cm^{-1}) 3427 (NH), 1729 (CO); ^{1}H NMR (DMSO-d_6): δ = 2.41 (s, 3H, CH_3), 7.37−8.03 (m, 10H, 9 Ar-H and vinylic-H), 8.75 (s, 1H, pyrazole-H), 13.70 (s, 1H, NH, D_2O exchangeable); ^{13}C NMR (DMSO-d_6): δ = 20.87, 116.37, 119.48, 126.59, 127.63, 128.02, 128.29, 128.72, 128.55, 129.63, 138.65, 138.81, 154.67, 170.31, 194.65; *m*/*z* (%) = 378 (18.1, M$^+$+1), 377 (76.2, M$^+$), 301 (8.20), 284 (58.8), 208 (17.9), 91 (19.9), 77 (100.0). Anal. calcd for $C_{20}H_{15}N_3OS_2$ (377.48): C, 63.64; H, 4.01; N, 11.13; S, 16.99. Found: C, 63.50; H, 4.20; N, 11.32; S, 16.84%.

*5.2.3. 5-[(3-(4-Methoxyphenyl)-1-phenyl-1H-pyrazol-4-yl)-methylene]-4-thioxo-2-thiazolidinone (**3c**).* Red crystals; 42%; mp 306 °C; IR (KBr, cm^{-1}) 3429 (NH), 1728 (CO); ^{1}H NMR (DMSO-d_6): δ = 3.85 (s, 3H, OCH_3), 7.08−8.37 (m, 10H, 9 Ar-H and vinylic-H), 8.74 (s, 1H, pyrazole-H), 13.73 (s, 1H, NH, D_2O exchangeable); *m*/*z* (%) = 394 (26.5, M$^+$+1), 393 (100.0, M$^+$), 300 (60.5), 224 (14.6), 104 (19.3), 77 (94.8). Anal. calcd for $C_{20}H_{15}N_3O_2S_2$ (393.48): C, 61.05; H, 3.84; N, 10.68; S, 16.30. Found: C, 61.21; H, 4.03; N, 10.41; S, 16.07%.

*5.2.4. 5-[(3-(4-Chlorophenyl)-1-phenyl-1H-pyrazol-4-yl)-methylene]-4-thioxo-2-thiazolidinone (**3d**).* Red crystals; 55%; mp 300 °C; IR (KBr, cm^{-1}) 3433 (NH), 1735 (CO);

https://doi.org/10.1021/acsomega.2c06954
ACS Omega 2023, 8, 5571−5592

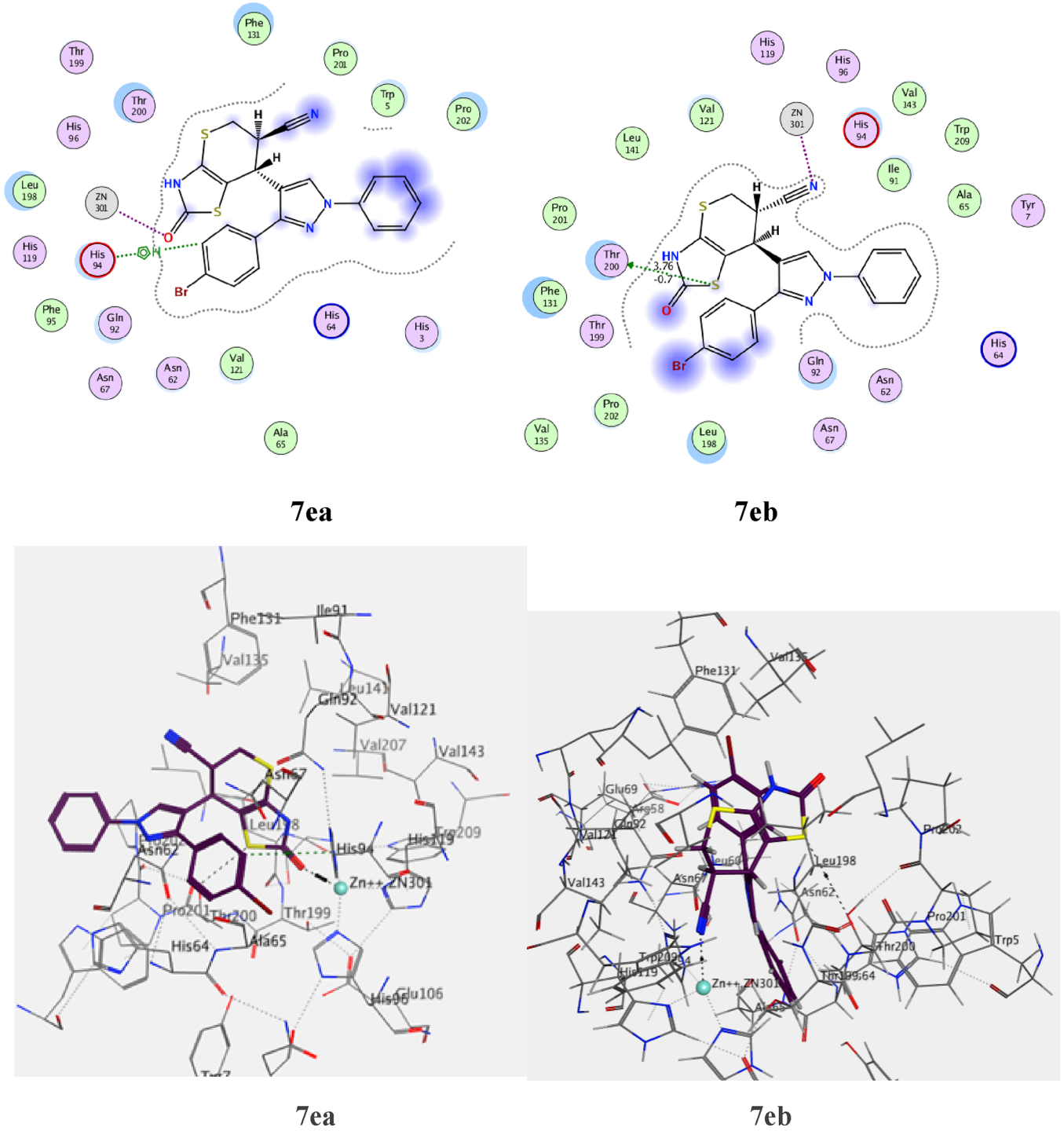

Figure 26. 2D and 3D ligand interaction of **7ea** and **7eb** with the amino acids of the 5U0F active site.

^{1}H NMR (DMSO-d_6): δ = 7.29−8.0 (m, 10H, 9 Ar-H and olefinic-H), 8.70 (s, 1H, pyrazole-H), 13.75 (s, 1H, NH, D_2O exchangeable); ^{13}C NMR (DMSO-d_6): δ = 116.40, 119.39, 125.71, 127.59, 127.99, 128.46, 129.26, 129.62, 130.02, 130.34, 133.98, 138.50, 139.1, 153.11, 170.20, 194.74; *m*/*z* (%) = 399 (31.8, M^++2), 398 (20.3, M^++1), 397 (69.1, M^+), 304 (46.9), 275 (12.5), 104 (17.6), 77 (100.0). Anal. calcd for $C_{19}H_{12}ClN_3OS_2$ (397.90): C, 57.35; H, 3.04; Cl, 8.91; N, 10.56; S, 16.12. Found: C, 57.14; H, 3.22; Cl, 9.05 N, 10.38; S, 15.96%.

*5.2.5. 5-[(3-(4-Bromophenyl)-1-phenyl-1H-pyrazol-4-yl)-methylene]-4-thioxo-2-thiazolidinone (**3e**).* Red crystals; 67%; mp >300 °C; IR (KBr, cm^{-1}) 3431 (NH), 1730 (CO); ^{1}H NMR (DMSO-d_6): δ = 7.26−8.01 (m, 10H, 9 Ar-H and olefinic-H), 8.71 (s, 1H, pyrazole-H), 13.73 (s, 1H, NH, D_2O exchangeable); *m*/*z* (%) = 443 (42.8, M^++2), 442 (15.6, M^++1), 441 (43.4, M^+), 350 (23.1), 348 (23.7), 275 (17.1), 231 (13.8), 104 (17.1), 77 (100.0). Anal. calcd for $C_{19}H_{12}BrN_3OS_2$ (442.35): C, 51.59; H, 2.73; Br, 18.06; N, 9.50; S, 14.50. Found: C, 51.33; H, 2.95; Br, 18.22; N, 9.22; S, 14.72%.

https://doi.org/10.1021/acsomega.2c06954
ACS Omega 2023, 8, 5571−5592

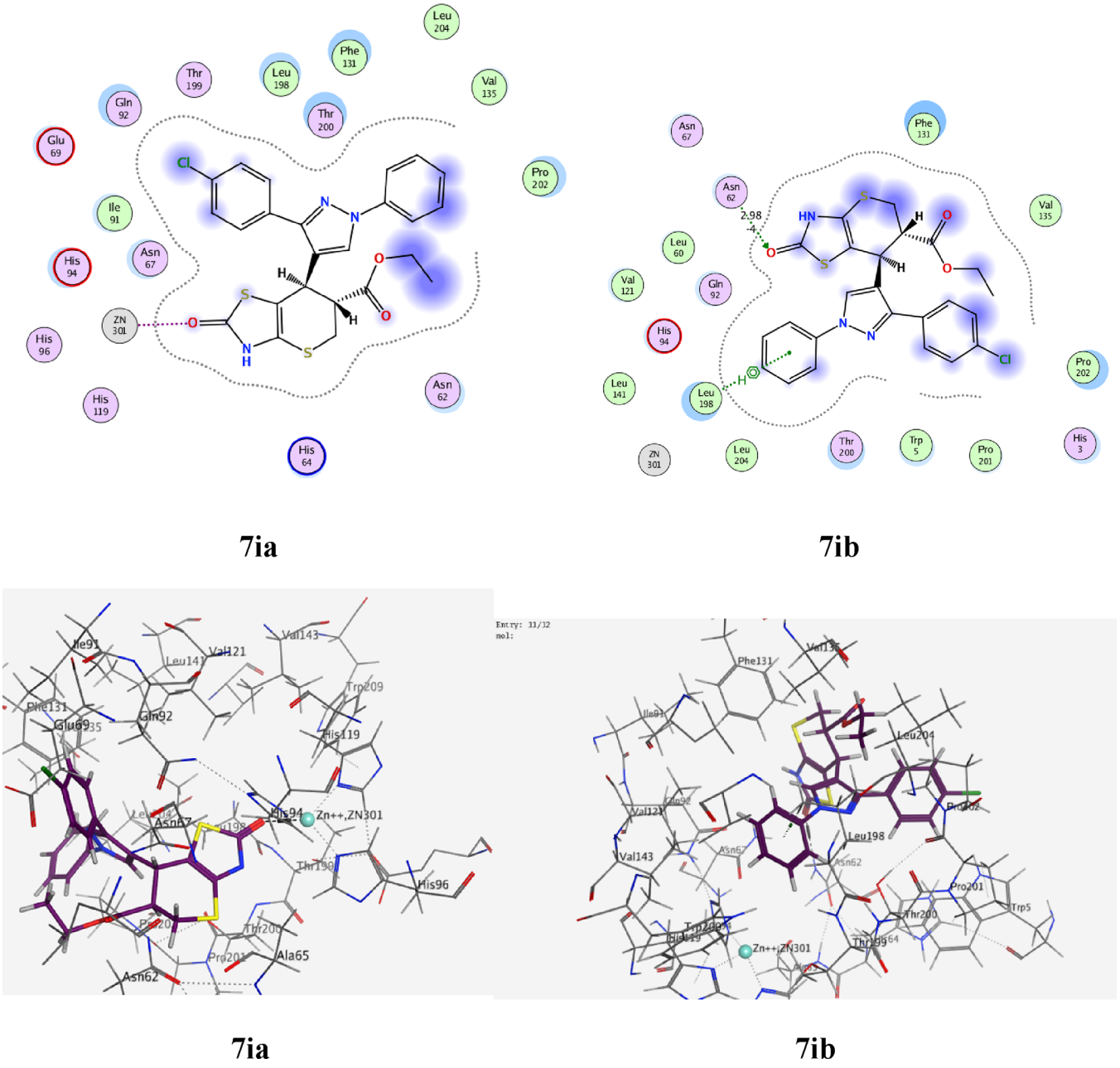

Figure 27. 2D and 3D ligand interaction of **7ia** and **7ib** with the amino acids of the 5U0F active site.

4.1.3. Synthesis of 8-(3-Aryl-1-phenyl-1H-pyrazol-4-yl)-6-arylpyrrolo[3′,4′:5,6]-thiopyrano[2,3-d]thiazole-2,5,7-trione 5a−g. **5.3. General Procedure.** *N*-Aryl maleimides **4a−c** were added to the suspension of the 5-arylmethylene-4-thioxo-2-thiazolidinone derivatives **3a−e** (0.01 mol) in glacial acetic acid (20 mL) (0.01 mol). The mixture was refluxed until decolorization occurred and was then left at room temperature for the night. The resulting solid product was filtered out and recrystallized from an ethanol and dioxane combination.

*5.3.1. 8-(1,3-Diphenyl-1H-pyrazol-4-yl)-6-phenyl-7a,8-dihydropyrrolo[3′,4′:5,6]-thiopyrano[2,3-d]thiazole-2,5,7-(3H,4aH,6H)-trione (**5a**).* Yellow crystals; 53%; mp 230 °C; IR (KBr, cm^{-1}) 3440 (NH), 1714, 1677 (CO); ^{1}H NMR (DMSO-d_6): δ = 4.34 (dd, 1H, J = 3.6 Hz, 8.7 Hz, H-6), 4.41 (d, 1H, J = 3.9 Hz, H-5), 4.98 (d, 1H, J = 8.4 Hz, H-7), 7.02−7.84 (m, 15H, Ar-H), 8.71 (s, 1H, pyrazole-H), 11.83 (s, 1H, NH, D_2O exchangeable). Anal. calcd for $C_{29}H_{20}N_4O_3S_2$ (536.62): C, 64.91; H, 3.76; N, 10.44; S, 11.95. Found: C, 64.72; H, 3.95; N, 10.76; S, 11.78%.

*5.3.2. 8-(1,3-Diphenyl-1H-pyrazol-4-yl)-6-(4-methoxyphenyl)-7a,8-dihydropyrrolo[3′,4′:5,6]-thiopyrano[2,3-d]-thiazole-2,5,7(3H,4aH,6H)-trione (**5b**).* White crystals; 89%; mp 232 °C; IR (KBr, cm^{-1}) 3440 (NH), 1714, 1677 (CO); ^{1}H NMR (DMSO-d_6): δ = 3.77 (s, 3H, OCH_3), 4.13 (dd, 1H, J = 3.0 Hz, 9 Hz, H-6), 4.90 (d, 1H, J = 2.7 Hz, H-5), 4.93 (d, 1H, J = 9 Hz, H-7), 7.03−7.98 (m, 14H, Ar-H), 8.60 (s, 1H, pyrazole-H), 11.73 (s, 1H, NH, D_2O exchangeable); ^{13}C NMR (DMSO-d_6): δ = 31.37, 40.06, 48.17, 55.36, 110.12, 114.34, 118.29, 118.66, 119.77, 124.34, 126.29, 127.81, 128.00, 128.30, 128.72, 129.44, 132.85, 139.36, 150.29, 159.19, 170.50, 174.70, 174.94. m/z (%) = 566 (0.32 M^+), 363 (100), 330 (2.29), 319 (5.38), 270 (0.43), 104 (5.05), 77 (27.82). Anal. calcd for

https://doi.org/10.1021/acsomega.2c06954
ACS Omega 2023, 8, 5571−5592

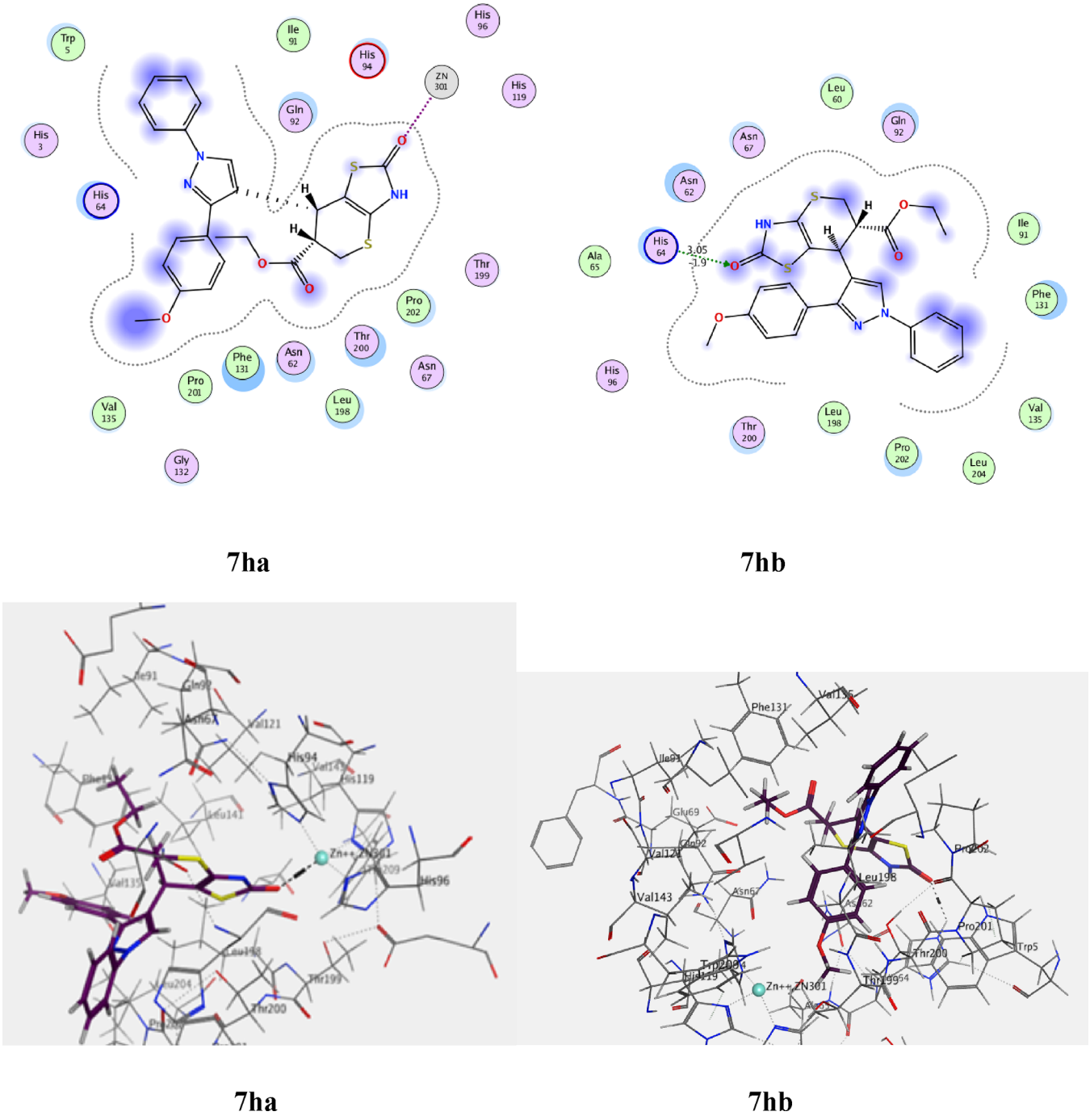

Figure 28. 2D and 3D ligand interaction of **7ha** and **7 hb** with the amino acids of the 5U0F active site.

$C_{30}H_{22}N_4O_4S_2$ (566.65): C, 63.59; H, 3.91; N, 9.89; S, 11.32. Found: C, 63.74; H, 3.76; N, 10.12; S, 11.09%.

*5.3.3. 6-(4-Chlorophenyl)-8-(1,3-diphenyl-1H-pyrazol-4-yl)-7a,8-dihydropyrrolo-[3′,4′:5,6]-thiopyrano[2,3-d]-thiazole-2,5,7(3H,4aH,6H)-trione (**5c**).* White crystals; 85%; mp 252 °C; IR (KBr, cm^{-1}) 3250 (NH), 1712, 1679, 1685 (CO); ^1H NMR (DMSO-d_6): δ = 4.11 (dd, 1H, J = 3.3 Hz, 9 Hz, H-6), 4.91−4.94 (m, 2H, H-5 and H-6), 7.17−7.96 (m, 14H, Ar-H), 8.57 (s, 1H, pyrazole-H), 11.70 (s, 1H, NH, D_2O exchangeable). ^{13}C NMR (DMSO-d_6): δ = 31.23, 42.92, 48.15, 109.93, 118.21, 118.46, 119.74, 126.25, 127.92, 128.33, 128.70, 129.18, 129.42, 130.54, 132.77, 133.20, 139.28, 143.92, 150.16, 170.47, 174.36, 174.57. m/z (%) = 572 (1.03, M^+ +1), 363 (97.74), 330 (2.52), 319 (5.87), 302 (2.06), 270 (1.20), 104 (4.81), 90 (8.04), 77 (100). Anal. calcd for $C_{29}H_{19}ClN_4O_3S_2$ (571.07): C, 60.99; H, 3.35; Cl, 6.21; N, 9.81; S, 11.23. Found: C, 60.68; H, 3.54; Cl, 6.40; N, 10.0; S, 11.02%.

*5.3.4. 8-(3-(4-Methylphenyl)-1-phenyl-1H-pyrazol-4-yl)-6-phenyl-7a,8-dihydro-pyrrolo[3′,4′:5,6]-thiopyrano[2,3-d]-thiazole-2,5,7(3H,4aH,6H)-trione (**5d**).* White crystals; 56%; mp 210 °C; IR (KBr, cm^{-1}) 3440 (NH), 1714, 1682, 16,677 (CO); ^1H NMR (DMSO-d_6): δ = 2.36 (s, 3H, CH_3), 4.35 (dd, 1H, J = 3.6 Hz, 8.4 Hz, H-6), 4.43 (d, 1H, J = 3.6 Hz, H-5), 4.98 (d, 1H, J = 8.4 Hz, H-7), 7.06−7.84 (m, 14H, Ar-H), 8.74 (s, 1H, pyrazole-H), 11.89 (s, 1H, NH, D_2O exchangeable); ^{13}C NMR (DMSO-d_6): δ = 20.77, 34.05, 46.31, 49.48, 66.33,

https://doi.org/10.1021/acsomega.2c06954
ACS Omega 2023, 8, 5571−5592

114.95, 116.92, 118.42, 119.55, 126.55, 126.60, 128.00, 128.65, 128.80, 129.12, 129.27, 129.47, 129.53, 129.63, 131.72, 137.71, 139.28, 151.71, 170.44, 174.00, 174.10. Anal. calcd for $C_{30}H_{22}N_4O_3S_2$ (550.65): C, 65.44; H, 4.03; N, 10.17; S, 11.65. Found: C, 65.27; H, 3.90; N, 10.39; S, 11.83%.

*5.3.5. 8-(3-(4-Methoxyphenyl)-1-phenyl-1H-pyrazol-4-yl)-6-phenyl-7a,8-dihydro-pyrrolo-[3′,4′:5,6]thiopyrano[2,3-d]-thiazole-2,5,7(3H,4aH,6H)-trione (**5e**).* Pale yellow crystals; 87%; mp 182 °C; IR (KBr, cm^{-1}) 3440 (NH), 1714, 1682 (CO); ^{1}H NMR (DMSO-d_6): δ = 3.81 (s, 3H, OCH_3), 4.20 (dd, 1H, J = 3.0 Hz, 9.0 Hz, H-6), 4.92 (d, 1H, J = 3.0 Hz, H-5), 4.94 (d, 1H, J = 9.0 Hz, H-7), 7.07−7.96 (m, 14H, Ar-H), 8.56 (s, 1H, pyrazole-H), 11.75 (s, 1H, NH, D_2O exchangeable); ^{13}C NMR (DMSO-d_6): δ = 31.42, 43.06, 48.15, 55.14, 110.16, 114.15, 116.80, 119.55, 119.71, 124.73, 125.20, 126.14, 128.14, 129.10, 129.41, 131.83, 139.40, 150.13, 159.32, 170.53, 174.52, 174.80; m/z (%) = 567 (4.8, M^++1), 566 (12.4, M^+), 522 (11.1), 435 (7.0), 393 (23.3), 173 (27.6), 104 (21.8), 77 (100.0). Anal. calcd for $C_{30}H_{22}N_4O_4S_2$ (566.65): C, 63.59; H, 3.91; N, 9.89; S, 11.32. Found: C, 63.41; H, 3.69; N, 10.20; S, 11.58%.

*5.3.6. 8-(3-(4-Chlorophenyl)-1-phenyl-1H-pyrazol-4-yl)-6-phenyl-7a,8-dihydro-pyrrolo[3′,4′:5,6]-thiopyrano[2,3-d]-thiazole-2,5,7(3H,4aH,6H)-trione (**5f**).* Yellow crystals; 85%; mp 251 °C; IR (KBr, cm^{-1}) 3250 (NH), 1695 (CO); ^{1}H NMR (DMSO-d_6): δ = 4.07 (dd, 1H, J = 3.3 Hz, 8.7 Hz, H-6), 4.84 (d, 1H, J = 8.7 Hz, H-7), 4.94 (d, 1H, J = 3.0 Hz, H-5), 7.11−7.58 (m, 12H, Ar-H), 7.79 (d, 1H, J = 8.4 Hz, Ar), 7.92 (d, 1H, J = 8.4 Hz, Ar), 8.55 (s, 1H, pyrazole-H), 11.70 (s, 1H, NH, D_2O exchangeable). ^{13}C NMR (DMSO-d_6): δ = 31.36, 43.12, 48.17, 109.92, 118.36, 118.64, 120.13, 126.47, 126.65, 128.68, 128.82, 129.18, 129.56, 129.78, 131.77, 131.84, 133.09, 139.28, 149.07, 170.61, 174.65, 174.83; m/z (%) = 572 (0.51, M^++1), 571 (0.47, M^+), 521 (0.17), 425 (0.11), 397 (100), 355 (1.94), 304 (3.38), 91 (6.62), 77 (85.09). Anal. calcd for $C_{29}H_{19}ClN_4O_3S_2$ (571.07): C, 60.99; H, 3.35; Cl, 6.21; N, 9.81; S, 11.23. Found: C, 61.22; H, 3.59; Cl, 6.02; N, 9.65; S, 11.08%.

*5.3.7. 8-(3-(4-Bromophenyl)-1-phenyl-1H-pyrazol-4-yl)-6-phenyl-7a,8-dihydro-pyrrolo[3′,4′:5,6]-thiopyrano[2,3-d]-thiazole-2,5,7(3H,4aH,6H)-trione (**5g**).* White crystals; 85%; mp 245 °C; IR (KBr, cm^{-1}) 3442 (NH), 1716, 1679 (CO); ^{1}H NMR (DMSO-d_6): δ = 4.05 (dd, 1H, J = 3.0 Hz, 8.7 Hz, H-6), 4.83 (d, 1H, J = 9 Hz, H-7), 4.42 (d, 1H, J = 2.7 Hz, H-5), 7.10−8.0 (m, 14H, Ar-H), 8.54 (s, 1H, pyrazole-H), 11.70 (s, 1H, NH, D_2O exchangeable). ^{13}C NMR (DMSO-d_6): δ = 31.7, 43.12, 48.16, 109.92, 118.36, 118.64, 120.15, 121.75, 126.65, 128.72, 128.82, 129.18, 129.54, 130.05, 129.78, 131.73, 131.84, 132.12, 139.27, 143.54, 144.41, 149.09, 170.62, 174.64, 174.84; m/z (%) = 616 (0.18, M^++1), 615 (0.14, M^+), 441 (4.81), 399 (1.66), 350 (3.68), 173 (3.03), 129 (2.10), 104 (4.53), 77 (100.0). Anal. calcd for $C_{29}H_{19}BrN_4O_3S_2$ (615.52): C, 56.59; H, 3.11; Br, 12.98; N, 9.10; S, 10.42. Found: C, 56.41; H, 3.00; Br, 13.22; N, 9.34; S, 10.18%.

*5.3.8. Synthesis of 7-(3-Aryl-1-phenyl-1H-pyrazol-4-yl)-2-oxo-3,5,6,7-tetrahydro-2H-thiopyrano[2,3-d]thiazole Derivatives **7a**−**j**.* **5.4. General Procedure.** Either acrylonitrile (**6a**) or ethyl acrylate (**6b**) was added to **3a**−**e** (0.01 mol), suspended in glacial acetic acid (20 mL) (0.01 mol). The mixture was refluxed until decolorization occurred followed by an overnight resting period at room temperature. The resulting solid product was filtered out and recrystallized from an ethanol and dioxane mixture.

*5.4.1. 7-(1,3-Diphenyl-1H-pyrazol-4-yl)-2-oxo-3,5,6,7-tetrahydro-2H-thiopyrano-[2,3-d]thiazole-6-carbonitrile (**7a**).* White crystals; 66%; mp 264 °C; IR (KBr, cm^{-1}) 3126 (NH), 2245 (CN), 1639 (CO); ^{1}H NMR (DMSO-d_6): δ = 3.45−3.66 (m, 2H, H-5), 3.98−4.03 (m, 1H, H-6), 4.50 (d, 1H, J = 5.4 Hz, H-7), 7.31−7.66 (m, 8H, Ar-H), 7.92 (d, 1H, J = 7.8 Hz, Ar-H), 8.60 (s, 1H, pyrazole-H), 11.49 (s, 1H, NH, D_2O exchangeable); ^{13}C NMR (DMSO-d_6): δ = 27.57, 32.08, 33.66, 105.63, 118.82, 119.24, 119.58, 120.49, 127.03, 128.80, 129.16, 129.99, 132.61, 139.59, 144.80, 144.89, 151.68, 170.55. Anal. calcd for $C_{22}H_{16}N_4OS_2$ (416.52): m/z (%) = 416 (29.02, M^+), 379 (2.14, M^+), 363 (100), 330 (7.04.92), 319 (12.08), 287 (6.49), 270 (36.84), 172 (2−08), 104 (14.26), 77 (65.16). C, 63.44; H, 3.87; N, 13.45; S, 15.40. Found: C, 63.70; H, 3.98; N, 13.26; S, 15.18%.

*5.4.2. 7-(3-(4-Methylphenyl)-1-phenyl-1H-pyrazol-4-yl)-2-oxo-3,5,6,7-tetra-hydro-2H-thiopyrano-[2,3-d]thiazole-6-carbonitrile (**7b**).* White crystals; 41%; mp 252 °C; IR (KBr, cm^{-1}) 3435 (NH), 2246 (CN), 1637 (CO); ^{1}H NMR (DMSO-d_6): δ = 2.37 (s, 3H, CH_3), 3.44−3.64 (m, 2H, H-5), 3.95−3.99 (m, 1H, H-6), 4.48 (d, 1H, J = 5.1 Hz, H-7), 7.29−7.35 (m, 3H, Ar-H), 7.48−7.53 (m, 4H, Ar-H), 7.90 (d, 2H, J = 7.4 Hz, Ar-H), 8.57 (s, 1H, pyrazole-H), 11.48 (s, 1H, NH, D_2O exchangeable); ^{13}C NMR (DMSO-d_6): δ = 20.90, 27.19, 31.71, 33.27, 105.29, 118.38, 118.87, 119.14, 120.08, 126.57, 128.30, 128.70, 129.36, 129.60, 137.78, 139.23, 144.70, 151.30, 170.18. Anal. calcd for $C_{23}H_{18}N_4OS_2$ (430.55): m/z (%) = 430 (3.65, M^+), 377 (11.33), 334 (1.70), 313 (1.67), 284 (2.23), 245 (4.11), 173 (1.39), 104 (3.27), 77 (100.0). C, 64.16; H, 4.21; N, 13.01; S, 14.90. Found: C, 63.96; H, 3.99; N, 13.22; S, 15.12%.

*5.4.3. 7-(3-(4-Methoxyphenyl)-1-phenyl-1H-pyrazol-4-yl)-2-oxo-3,5,6,7-tetra-hydro-2H-thiopyrano[2,3-d]thiazole-6-carbonitrile (**7c**).* White crystals; 46%; mp 274 °C; IR (KBr, cm^{-1}) 3440 (NH), 2243 (CN), 1639 (CO); ^{1}H NMR (DMSO-d_6): δ = 3.81 (s, 3H, OCH_3), 3.42−3.61 (m, 2H, H-5), 3.96−4.01 (m, 1H, H-6), 4.50 (d, 1H, J = 5.1 Hz, H-7), 7.32−7.94 (m, 9H, Ar-H), 8.64 (s, 1H, pyrazole-H), 11.47 (s, 1H, NH, D_2O exchangeable); ^{13}C NMR (DMSO-d_6): δ = 27.03, 31.55, 33.12, 55.1, 104.96, 118.44, 118.81, 119.33, 120.21, 126.83, 128.80, 129.22, 129.64, 130.02, 131.15, 133.24, 139.17, 150.23, 170.12. Anal. calcd for $C_{23}H_{18}N_4O_2S_2$ (446.54): C, 61.86; H, 4.06; N, 12.55; S, 14.36. Found: C, 61.99; H, 3.85; N, 13.78; S, 14.19%.

*5.4.4. 7-(3-(4-Chlorophenyl)-1-phenyl-1H-pyrazol-4-yl)-2-oxo-3,5,6,7-tetra-hydro-2H-thiopyrano[2,3-d]thiazole-6-carbonitrile (**7d**).* White crystals; 44%; mp 300 °C; IR (KBr, cm^{-1}) 3442 (NH), 2245 (CN), 1644 (CO); ^{1}H NMR (DMSO-d_6): δ = 3.44−3.64 (m, 2H, H-5), 3.99−4.04 (m, 1H, H-6), 4.53 (d, 1H, J = 5.1 Hz, H-7), 7.32−7.72 (m, 2H, Ar-H), 7.49−7.52 (m, 1H, Ar-H), 7.53 (d, 2H, J = 7.5 Hz, Ar-H), 7.66 (d, 2H, J = 7.8 Hz, Ar-H), 7.92 (d, 2H, J = 7.2 Hz, Ar-H) 8.61 (s, 1H, pyrazole-H), 11.49 (s, 1H, NH, D_2O exchangeable); ^{13}C NMR (DMSO-d_6): δ = 27.02, 31.54, 33.13, 104.92, 118.43, 118.70, 119.21, 120.11, 126.66, 128.69, 128.99, 129.51, 130.07, 131.04, 133.09, 139.05, 149.99, 170.05; m/z (%) = 452 (4.2, M^++2), 451 (2.7, M^++1), 450 (9.8, M^+), 397 (70.5), 304 (43.5), 104 (18.2), 77 (100.0). Anal. calcd for $C_{22}H_{15}ClN_4OS_2$ (450.96): C, 58.59; H, 3.35; Cl, 7.86; N, 12.42; S, 14.22. Found: C, 58.36; H, 3.18; Cl, 7.99; N, 12.65; S, 14.41%.

*5.4.5. 7-(3-(4-Bromophenyl)-1-phenyl-1H-pyrazol-4-yl)-2-oxo-3,5,6,7-tetrahydro-2H-thiopyrano-[2,3-d]thiazole-6-carbonitrile (**7e**).* White crystals; 42%; mp 299 °C; IR (KBr,

https://doi.org/10.1021/acsomega.2c06954
ACS Omega 2023, 8, 5571−5592

cm^{-1}) 3441 (NH), 2246 (CN), 1647 (CO); ^{1}H NMR (DMSO-d_6): δ = 3.43−3.50 (m, 1H, H-5), 3.59−3.64 (m, 1H, H-5), 3.96−3.99 (m, 1H, H-6), 4.51 (d, 1H, J = 5.4 Hz, H-7), 7.32−8.02 (m, 9H, Ar-H), 8.76 (s, 1H, pyrazole-H), 11.49 (s, 1H, NH, D_2O exchangeable). m/z (%) = 496 (3.21, M$^+$+1), 495 (1.38, M$^+$), 459 (1.19), 443 (53.64), 382 (3.61), 350 (26.66), 319 (10.09), 275 (14.67), 231 (8.98), 181 (5.22), 172 (4.38), 129 (6.47), 104 (15.09), 77 (100.0). Anal. calcd for $C_{22}H_{15}BrN_4OS_2$ (495.41): C, 53.34; H, 3.05; Br, 16.13; N, 11.31; S, 12.94. Found: C, 53.50; H, 3.20; Br, 15.96; N, 11.21; S, 12.75%.

*5.4.6. Ethyl 7-(1,3-Diphenyl-1H-pyrazol-4-yl)-2-oxo-3,5,6,7-tetrahydro-2H-thiopyrano[2,3-d]thiazole-6-carboxylate (**7f**).* White crystals; 71%; mp 242 °C; IR (KBr, cm^{-1}) 3433 (NH), 1725, 1649 (CO); ^{1}H NMR (DMSO-d_6): δ = 0.69 (t, 3H, J = 7.2 Hz, $CH_2\underline{CH_3}$), 3.16−3.29 (m, 2H, H-5), 3.46−3.50 (m, 1H, H-6), 3.76 (q, 2H, J = 7.2 Hz, $\underline{CH_2}CH_3$), 4.56 (d, 1H, J = 5.4 Hz, H-7), 7.31−7.60 (m, 8H, Ar-H), 7.92−7.95 (m, 2H, Ar-H), 8.58 (s, 1H, pyrazole-H), 11.38 (s, 1H, NH, D_2O exchangeable); ^{13}C NMR (DMSO-d_6): δ = 13.33, 23.54, 30.51, 45.01, 60.30, 106.38, 118.17, 119.48, 120.05, 126.37, 128.11, 128.31, 128.52, 128.66, 129.45, 132.83, 139.19, 144.12, 144.22, 150.99, 170.61. m/z (%) = 463 (6.49, M$^+$), 363 (27.97), 319 (7.41), 302 (8.63), 270 (15.69), 171 (1.91), 104 (13.62), 77 (100.0). Anal. calcd for $C_{24}H_{21}N_3O_3S_2$ (463.10): C, 62.18; H, 4.57; N, 9.06; S, 13.83. Found: C, 61.98; H, 4.25; N, 9.32; S, 14.02%.

*5.4.7. Ethyl 7-(3-(4-Methylphenyl)-1-phenyl-1H-pyrazol-4-yl)-2-oxo-3,5,6,7-tetrahydro-2H-thiopyrano[2,3-d]thiazole-6-carboxylate (**7g**).* White crystals; 45%; mp 252 °C; IR (KBr, cm^{-1}) 3447 (NH), 1731, 1678 (CO); ^{1}H NMR (DMSO-d_6): δ = 0.741 (t, 3H, J = 6.9 Hz, $CH_2\underline{CH_3}$), 2.36 (s, 3H, CH_3), 3.12−3.33 (m, 2H, H-5), 3.47−3.52 (m, 1H, H-6), 3.75 (q, 2H, J = 6.9 Hz, $\underline{CH_2}CH_3$), 4.55 (d, 1H, J = 5.1 Hz, H-7), 7.29 (d, 2H, J = 7.5 Hz, Ar-H), 7.31−7.50 (m, 5H, Ar-H), 7.91 (d, 2H, J = 7.8 Hz, Ar-H), 8.56 (s, 1H, pyrazole-H), 11.39 (s, 1H, NH, D_2O exchangeable); ^{13}C NMR (DMSO-d_6): δ = 13.22, 20.75, 23.62, 30.52, 44.98, 60.25, 106.42, 118.08, 119.33, 119.92, 126.16, 128.14, 128.26, 129.07, 129.32, 129.93, 137.35, 139.20, 150.99, 170.47. Anal. calcd for $C_{25}H_{23}N_3O_3S_2$ (477.12): C, 62.87; H, 4.85; N, 8.80; S, 13.43. Found: C, 62.74; H, 4.99; N, 9.00; S, 13.21%.

*5.4.8. Ethyl 7-(3-(4-Methoxyphenyl)-1-phenyl-1H-pyrazol-4-yl)-2-oxo-3,5,6,7-tetrahydro-2H-thiopyrano[2,3-d]thiazole-6-carboxylate (**7h**).* White crystals; 84%; mp 250 °C; IR (KBr, cm^{-1}) 3444 (NH), 1736, 1640 (CO); ^{1}H NMR (DMSO-d_6): δ = 0.73 (t, 3H, J = 6.9 Hz, $CH_2\underline{CH_3}$), 3.13−3.35 (m, 2H, H-5), 3.49−3.53 (m, 1H, H-6), 3.77−3.83 (m, 5H, OCH_3 and $\underline{CH_2}CH_3$), 4.55 (d, 1H, J = 5.1 Hz, H-7), 7.05 (d, 2H, J = 8.7 Hz, Ar-H), 7.26−7.54 (m, 5H, Ar-H), 7.91 (d, 2H, J = 8.1 Hz, Ar-H), 8.54 (s, 1H, pyrazole-H), 11.39 (s, 1H, NH, D_2O exchangeable); ^{13}C NMR (DMSO-d_6): δ = 13.31, 23.68, 30.59, 45.02, 55.14, 60.29, 106.51, 114.01, 118.07, 119.32, 119.83, 125.19, 126.12, 128.17, 129.33, 129.53, 139.25, 150.86, 159.18, 170.53; m/z (%) = 494 (5.7, M$^+$+1), 493 (17.5, M$^+$), 393 (100.0), 300 (54.3), 224 (13.4), 104 (17.7) 77 (73.7). Anal. calcd for $C_{25}H_{23}N_3O_4S_2$ (493.11): C, 60.83; H, 4.70; N, 8.51; S, 12.99. Found: C, 60.99; H, 4.63; N, 8.74; S, 12.78%.

*5.4.9. Ethyl 7-(3-(4-Chlorophenyl)-1-phenyl-1H-pyrazol-4-yl)-2-oxo-3,5,6,7-tetra-hydro-2H-thiopyrano[2,3-d]thiazole-6-carboxylate (**7i**).* White crystals; 41%; mp 254 °C; IR (KBr, cm^{-1}) 3117 (NH), 1735, 1640 (CO); ^{1}H NMR (DMSO-d_6): δ = 0.73 (t, 3H, J = 6.9 Hz, $CH_2\underline{CH_3}$), 3.12−3.38 (m, 2H, H-5), 3.46−3.55 (m, 1H, H-6), 3.75 (q, 2H, J = 6.9 Hz, $\underline{CH_2}CH_3$), 4.52 (d, 1H, J = 5.4 Hz, H-7), 7.05 (d, 2H, J = 9 Hz, Ar-H), 7.27−7.32 (m, 1H, Ar-H), 7.45−7.53 (m, 4H, Ar-H), 7.90 (d, 2H, J = 7.8 Hz, Ar-H), 8.54 (s, 1H, pyrazole-H), 11.37 (s, 1H, NH, D_2O exchangeable); ^{13}C NMR (DMSO-d_6): δ = 13.76, 24.04, 30.96, 45.41, 60.73, 106.91, 114.47, 118.48, 119.77, 120.26, 125.57, 126.60, 128.65, 129.82, 129.96, 139.65, 144.16, 151.25, 159.59, 170.07. Anal. calcd for $C_{24}H_{20}ClN_3O_3S_2$ (497.99): C, 57.88; H, 4.05; Cl, 7.12; N, 8.44; S, 12.88. Found: C, 57.56; H, 3.89; Cl, 7.36; N, 8.78; S, 12.62%.

*5.4.10. Ethyl 7-(3-(4-Bromophenyl)-1-phenyl-1H-pyrazol-4-yl)-2-oxo-3,5,6,7-tetra-hydro-2H-thiopyrano[2,3-d]thiazole-6-carboxylate (**7j**).* White crystals; 41%; mp 256 °C; IR (KBr, cm^{-1}) 3447 (NH), 1732, 1679 (CO); ^{1}H NMR (DMSO-d_6): δ = 0.73 (t, 3H, J = 6.9 Hz, $CH_2\underline{CH_3}$), 3.12−3.29 (m, 2H, H-5), 3.43−3.47 (m, 1H, H-6), 3.75 (q, 2H, J = 6.9 Hz, $\underline{CH_2}CH_3$), 4.54 (d, 1H, J = 5.4 Hz, H-7), 7.29−7.99 (m, 9H, Ar-H), 8.65 (s, 1H, pyrazole-H), 11.39 (s, 1H, NH, D_2O exchangeable). m/z (%) = 543 (0.93, M$^+$+1), 542 (0.41, M$^+$), 441 (3.40), 348 (2.16), 319 (0.85), 275 (1.25), 231 (1.27), 155 (1.24), 104 (5.33), 77 (100.0). Anal. calcd for $C_{24}H_{20}BrN_3O_3S_2$ (542.47): C, 53.14; H, 3.72; Br, 14.73; N, 7.75; S, 11.82. Found: C, 53.32; H, 3.95; Br, 14.63; N, 7.56; S, 11.99%.

5.5. Crystallographic Analysis. To determine the three dimensional structure of the titled structure, a study was conducted. Below is a table of geometries. MaXus was used to complete computations and draw various diagrams (Bruker Nonius, Delft and MacScience, Japan).

Crystal data for **5a**: $C_{29}H_{20}N_4O_3S_2$, = M_r = 536.632, triclinic, a = 8.4142(3), b = 10.5253(4), c = 14.5668(6) Å, α = 90.911 (2)°, β = 100.943(2)°, γ = 95.418(3)°, V = 1260.19(8) Å^3, Z = 2, D_x = 1.414 Mg/m^{-3}, Mo Kα radiation, λ = 0.71073 Å, Cell parameters from 2935, T = 298 K, θ = 2.910−27.485°, θ_{max} = 27.57°, R_{int} = 0.030. Refinement on F^2; R(all) = 0.133, R(gt) = 0.039, wR(ref) = 0.069, wR(all) = 0.098, wR(gt) = 0.069. S(ref) = 1.224, S(all) = 1.198, S(gt) = 1.228, 2557 reflections and 343 parameters, μ = 0.25 mm^{-1}. Deposition number (CCDC) 1544355. The Cambridge Crystallographic Data Centre (CCDC), 12 Union Road, Cambridge CB2 1EZ, UK; fax: +44 (0) 1223 336,033; email: deposit@ccdc.cam.ac.uk, is where you can get these data for free (see Supporting Information).

6. MATERIALS AND METHODS

BIOLOGICAL ACTIVITY METHODSHOLDING COMPANY FOR BIOLOGICAL PRODUCTS AND VACCINES (VACSERA), CAIRO, EGYPT, RECEIVED THE HUMAN NORMAL LUNG FIBROBLAST (WI38), HEPATOCELLULAR CARCINOMA (HEPG-2), AND MAMMARY GLAND BREAST CANCER (MCF-7) CELL LINES FROM ATCC AND EMPLOYED DOXORUBICIN AS A STANDARD DRUG.

6.1. MTT Assay. The MTT test was performed to assess the inhibitory effect of the substances on cell growth in the aforementioned cell lines. This colorimetric technique relies on mitochondrial succinate dehydrogenase, which transforms the yellow tetrazolium bromide (MTT) into a purple formazan

https://doi.org/10.1021/acsomega.2c06954
ACS Omega 2023, 8, 5571−5592

derivative in living cells. A 10% fetal bovine serum was added to RPMI-1640 medium in which cell lines were grown.

The cells were grown in a 5% CO_2 incubator at 37 °C with addition of antibiotics (100 units/mL penicillin and 100 g/mL streptomycin). Under 96-well plates, cell lines were seeded at a density of 1.0 × 104 cells/well for 48 h. Then, the cells were exposed to various concentrations of compounds and incubated for 24 h. For 4 h, 20 μL of a 5 mg/mL MTT solution was incubated and then underwent drug treatment for 24 h. Each well received 100 μ of DMSO to dissolve the purple formazan. A plate reader was used to measure and record the absorbance at 570 nm (EXL 800, USA). The relative cell viability percentage was determined as (A570 of the treated sample/A570 of the untreated sample) times 100.[66,67]

6.2. Enzyme Inhibition. *h*CAIX and *h*CAXII enzyme inhibition assay was performed: human carbonic anhydrase IX (hCAIX), containing a C-terminal His-tag, MW = 40 kDa, produced in an Sf9 cell expression system infected with a baculovirus 1400 pmol/min/g of specific activity; recombinant human carbonic anhydrase XII (*h*CAXII) source from the mouse myeloma cell line, NS0-derived Ala25Gln291, with a *C*-terminal 10His tag *N*-terminal Sequence Analysis Ala25 (see Supporting Information).

6.3. Method. *p*-Nitrophenyl acetate is hydrolyzed through CA to produce *p*-nitrophenol. The intensity of the yellow color of *p*-nitrophenol is proportional to the amount of the substrate, *p*-nitrophenyl acetate buffer 0.1 M (pH 7.4). After incubation at room temperature for 3 min, the absorbance of the sample at 348 nm was measured using a spectrophotometer. A standard curve was derived from a series of *p*-nitrophenol solutions ranging from 0 to 100 nmol/mL[68,69] (see Supporting Information).

6.4. *In Vitro* Cell Cycle Analysis. *In vitro* cell cycle analysis: HePG-2 cells are precultured in a 25 cm^2 cell culture flask. The investigated chemicals **7e** and **7i** were utilized in the cell treatment at their IC_{50} values after being individually dissolved in the necessary medium, which was RPMI-1640. Cells were extracted after an overnight treatment, carefully fixed with 70% (v/v) ethanol in PBS and then suspended in PBS containing 40 g/mL propidium iodide (PI), 0.1 mg/mL RNase, and 0.1% (v/v) Triton X-100 in a darkened room. A flow cytometer fitted with an argon-ion laser at a wavelength of 488 nm was used to analyze the cell cycle after 30 min at 37 °C and quantify the proportion of cells in G1, S, and G2/M.

6.5. Annexin V-FITC Apoptosis Assay. HePG-2 cells were collected and treated with **7e** and **7i** individually for 48 h in the annexin V FITC apoptosis test. The cells were then collected, repeatedly rinsed with PBS twice, and centrifuged. After that, using the apoptosis detection kit (BD Biosciences, San Jose, CA) in accordance with the manufacturer's instructions, the cells were treated with annexin V-FITC and propidium iodide (PI). A flow cytometer was used to examine PI binding and annexin V-FITC binding.

6.6. Western Blot Analysis. According to the above-mentioned information of the most potent inhibitors **7e** and **7i** against CAIX and CAXII, a further study was carried out as Western Blot analysis in gel electrophoresis and immunoblot analysis of proteins.[70,71]

6.7. Method. To separate proteins according to their sizes, sodium dodecyl sulfate polyacrylamide gel electrophoresis is employed. It is generally used in conjunction with western blotting (immunoblotting) to establish the presence and/or relative abundance of a target protein in a sample containing a complex protein combination. In this approach, the total protein in each sample is loaded, and then using an electric current to transport the proteins through the gel matrix, the samples are electrophoretically separated. The proteins must first come into touch with a detergent as SDS, which denatures and negatively charges the proteins. A molecular weight marker that generates bands of known size is used to help identify the protein of interest. Once the proteins separated, an electric current is used to transfer the gel to a polyvinylidene fluoride membrane, allowing the proteins to migrate from the gel onto the membrane. A secondary antibody that binds to the complex *via* its antibody side is added in order to detect a specific protein on the membrane after a primary antibody to that protein has been added to form a protein−antibody complex. Most frequently, the secondary antibody is joined to an enzyme that reacts with the substrate to produce light. The Biorad Imager can record this luminescence, which is proportional to the volume of the protein that interacted with the antibody. The chemical technique is in the Supporting Information.

6.8. Molecular Docking. Molecular Operating Environment (MOE) software version 2015.10[72] was used for the molecular docking study. The original ligand is present in the CA IX and CA XII X-ray crystal structures (PDB: 5U0F) [(5*R*)-5-[(2,4-dimethoxyphenyl)methyl]-2-sulfanylidene-1,3-thiazolidin-4].[73] Protein was prepared *via* 3D protonation; the water molecules and ligand that were not implicated in the active site were removed; and the default protocol was then used to build the active site. Then, hydrogen atoms were added to the protein and reduced until the RMS gradient and RMS distance were both 0.01 kcal mol^{-1} and 0.1, respectively. London dG was chosen as the docking score energy and triangular matcher as the placement technique. The original ligand, AZA, self-docked in the active site to start the docking process. The compounds **7e** and **7i** were generated from Chemdraw 14.0, then subjected to 3D protonation with minimized energy, and saved as an mdb file as a ligand atom that was then used in the docking protocol and then replaced the co-crystallized AZA under the same methods.

■ ASSOCIATED CONTENT

Supporting Information

The Supporting Information is available free of charge at https://pubs.acs.org/doi/10.1021/acsomega.2c06954.

All spectral data such as IR, ^{1}H NMR, ^{13}C NMR, and IR for newly synthesized compounds and raw data for the biological part (PDF)

■ AUTHOR INFORMATION

Corresponding Author

Nadia Hanafy Metwally − *Chemistry Department, Faculty of Science, Cairo University, Giza 12613, Egypt*; orcid.org/0000-0002-9706-3694; Email: mnadia@sci.cu.edu.eg

Author

Ebrahim Adel El-Desoky − *Chemistry Department, Faculty of Science, Cairo University, Giza 12613, Egypt*

Complete contact information is available at: https://pubs.acs.org/10.1021/acsomega.2c06954

Notes

The authors declare no competing financial interest.

https://doi.org/10.1021/acsomega.2c06954
ACS Omega 2023, 8, 5571−5592

REFERENCES

(1) Pouyssegur, J.; Dayan, F.; Mazure, N. M. Hypoxia signalling in cancer and approaches to enforce tumour regression. *Nature* **2006**, *441*, 437−443.

(2) Neri, D.; Supuran, C. T. Interfering with pH regulation in tumours as a therapeutic strategy. *Nat. Rev. Drug Discovery* **2011**, *10*, 767−777.

(3) Supuran, C. T. Carbonic anhydrases: novel therapeutic applications for inhibitors and activators. *Nat. Rev. Drug Discovery* **2008**, *7*, 168−181.

(4) Chiche, J.; Ilc, K.; Laferriére, J.; Trottier, E.; Dayan, F.; Mazure, N. M.; Horn, M. C. B.; Pouyssegur, J. Hypoxia-inducible carbonic anhydrase IX and XII promote tumor cell growth by counteracting acidosis through the regulation of the intracellular pH. *Cancer Res.* **2009**, *69*, 358−368.

(5) Kallio, H.; Rodriguez, A. M.; Hilvo, M.; Hyrskyluoto, A.; Parkkila, S. Cancer-associated carbonic anhydrases IX and XII: effect of growth factors on gene expression in human cancer cell lines. *J. Cancer Mol.* **2010**, *5*, 73−78.

(6) Ondriskova, E.; Debreova, M.; Pastorekova, S. Tumor-associated carbonic anhydrases IX and XII. In: Supuran, CT; De Simone, G, editors. *Carbonic anhydrases as biocatalysts from theory to medical and industrial applications*; Elsevier: Amsterdam 2015; pp. 169−205.

(7) Kuijk, S. J. V.; Yaromina, A.; Houben, R.; Niemans, R.; Lambin, P.; Dubois, L. J. Prognostic significance of carbonic anhydrase IX expression in cancer patients: a meta-analysis. *Front. Oncol.* **2016**, *6*, 69.

(8) Kciuk, M.; Gielecinska, A.; Mujwar, S.; Mojzych, M.; Marciniak, B.; Drozda, R.; Kontek, R. Targeting carbonic anhydrase IX and XII isoforms with small molecule inhibitors and monoclonal antibodies. *J. Enzyme Inhib. Med. Chem.* **2022**, *37*, 1278−1298.

(9) Supuran, C. T. Structure and function of carbonic anhydrases. *Biochem. J.* **2016**, *473*, 2023−2032.

(10) Boone, C. D.; Pinard, M.; McKenna, R.; Silverman, D. Catalytic mechanism of α-class carbonic anhydrases: CO_2 hydration and proton transfer. *Subcell. Biochem.* **2014**, *75*, 31−52.

(11) McKenna, R.; Supuran, C. T. Carbonic anhydrase inhibitors drug design. *Subcell. Biochem.* **2014**, *75*, 291−323.

(12) Supuran, C. T. Structure-based drug discovery of carbonic anhydrase inhibitors. *J. Enzyme Inhib. Med. Chem.* **2012**, *27*, 759−772.

(13) Tonissen, K. F.; Poulsen, S. A. Carbonic anhydrase XII inhibition overcomes P-glyco-protein-mediated drug resistance: a potential new combination therapy in cancer. *Cancer Drug Resist.* **2021**, *4*, 343−355.

(14) Frost, S. C.; McKenna, R. *Carbonic anhydrase: Mechanism, regulation, links to disease, and industrial applications. Subcellular Biochemistry*; Springer: Berlin/Heidelberg, Germany, 2014.

(15) Pinard, M. A.; Mahon, B.; McKenna, R. Probing the surface of human carbonic anhydrase for clues towards the design of isoform specific inhibitors. *BioMed Res. Int.* **2015**, *2015*, 1−15.

(16) Mboge, M. Y.; McKenna, R.; Frost, S. C. Advances in anti-cancer drug development targeting carbonic anhydrase IX and XII. *In Topics in Anti-Cancer Research*; Bentham Science Publishers: Sharjah, United Arab Emirates. 2016, *5*, 3−42, DOI: 10.2174/9781681083339116050004.

(17) Li, Y.; Tu, C.; Wang, H.; Silverman, D. N.; Frost, S. C. Catalysis and pH control by membrane-associated carbonic anhydrase IX in MDA-MB-231 breast cancer cells. *J. Biol. Chem.* **2011**, *286*, 15789−15796.

(18) Mahon, B. P.; Bhatt, A.; Socorro, L.; Driscoll, J. M.; Okoh, C.; Lomelino, C. L.; Mboge, M. Y.; Kurian, J. J.; Tu, C.; Agbandje-McKenna, M.; Frost, S. C.; McKenna, R. The structure of carbonic anhydrase IX is adapted for low-pH catalysis. *Biochemistry* **2016**, *55*, 4642−4653.

(19) Lounnas, N.; Rosilio, C.; Nebout, M.; Mary, D.; Griessinger, E.; Neffati, Z.; Chiche, J.; Spits, H.; Hagenbeek, T. J.; Asnafi, V.; Poulsen, S. A.; Supuran, C. T.; Peyron, J. F.; Imbert, V. Pharmacological inhibition of carbonic anhydrase XII interferes with cell proliferation and induces cell apoptosis in T-cell lymphomas. *Cancer Lett.* **2013**, *333*, 76−88.

(20) Yang, J. S.; Lin, C. W.; Chuang, C. Y.; Su, S. C.; Lin, S. H.; Yang, S. F. Carbonic anhydrase IX overexpression regulates the migration and progression in oral squamous cell carcinoma. *Tumour Biol. J. Int. Soc. Oncodev. Biol. Med.* **2015**, *36*, 9517−9524.

(21) Hsieh, M. J.; Chen, K. S.; Chiou, H. L.; Hsieh, Y. S. Carbonic anhydrase XII promotes invasion and migration ability of MDA-MB-231 breast cancer cells through the p38 MAPK signaling pathway. *Eur. J. Cell Biol.* **2010**, *89*, 598−606.

(22) Pacchiano, F.; Carta, F.; McDonald, P. C.; Lou, Y.; Vullo, D.; Scozzafava, A.; Dedhar, S.; Supuran, C. T. Ureido-substituted benzenesulfonamides potently inhibit carbonic anhydrase IX and show antimetastatic activity in a model of breast cancer metastasis. *J. Med. Chem.* **2011**, *54*, 1896−1902.

(23) Sugrue, M. F. Pharmacological and ocular hypotensive properties of topical carbonic anhydrase inhibitors. *Prog. Retin. Eye Res.* **2000**, *19*, 87−112.

(24) Asiedu, M.; Ossipov, M. H.; Kaila, K.; Price, T. J. Acetazolamide and midazolam act synergistically to inhibit neuropathic pain. *Pain.* **2010**, *148*, 302−308.

(25) Carta, F.; Cesare, L. M. D.; Pinard, M.; Ghelardini, C.; Scozzafava, A.; McKenna, R.; Supuran, C. T. A class of sulfonamide carbonic anhydrase inhibitors with neuropathic pain modulating effects. *Bioorg. Med. Chem.* **2015**, *23*, 1828−1840.

(26) Lesyk, R. Drug design: 4-thiazolidinones applications. Part 2. Pharmacological profiles. *J Med. Sci.* **2020**, *89*, No. e407.

(27) Lesyk, R. B.; Zimenkovsky, B. S.; Kaminskyy, D. V.; Kryshchyshyn, A. P.; Havrylyuk, D. Y.; Atamanyuk, D. V.; Subtelna, I. Y.; Khylyuk, D. V. Thiazolidinone motif in anticancer drug discovery. Experience of DH LNMU medicinal chemistry scientific group. *Biopolym. Cell* **2011**, *27*, 107−117.

(28) Agrawal, N. Synthetic and therapeutic potential of 4-thiazolidinone and its analogs. *Curr. Chem. Lett.* **2021**, *10*, 119−138.

(29) Mueller, S. L.; Chrysanthopoulos, P. K.; Halili, M. A.; Hepburn, C.; Nebl, T.; Supuran, C. T.; Nocentini, A.; Peat, T. S.; Poulsed, S.-A. The Glitazone class of drugs as carbonic anhydrase. *Molecules* **2021**, *26*, 3010.

(30) Palla, R.; Distratis, C.; Cominotto, R.; Panichi, V.; Pozzetti, G.; Bionda, A.; Neri, M.; Frattarelli, L.; Renal effects of etozolin in man. In *diuretics: Basic, pharmacological, and clinical Aspects. Developments in Nephrology*; Andreucci, V. E.; Dal Canton, A., Eds.; Springer: Boston, MA, USA, 1987; *18*, 553−555, ISBN 978−1−4612-9227-2.

(31) Bayindir, S.; Caglayan, C.; Karaman, M.; Gülcin, İ. The green synthesis and molecular docking of novel *N*-substituted rhodanines as effective inhibitors for carbonic anhydrase and acetylcholinesterase enzymes. *Bioorg. Chem.* **2019**, *90*, No. 103096.

(32) Pancholia, S.; Dhameliya, T. M.; Shah, P.; Jadhavar, P. S.; Sridevi, J. P.; Yogeshwari, P.; Sriram, D.; Chakraborti, A. K. 3-Benzo[*d*]thiazol-2-yl(piperazin-1-yl)methanones as new anti-mycobacterial chemotypes: Design, synthesis, biological evaluation and 3D-QSAR studies. *Eur. J. Med. Chem.* **2016**, *116*, 187−199.

(33) Dhameliya, T. M.; Patel, K. I.; Tiwari, R.; Vagolu, S. K.; Panda, D.; Sriram, D.; Chakraborti, A. K. Design, synthesis, and biological evaluation of benzo[*d*]imidazole-2-carboxamides as new anti-TB agents. *Bioorg. Chem.* **2021**, *107*, No. 104538.

(34) Kapileswar, S.; Garg, S. K.; Raj, R.; Priyank, P.; Meena, V. S.; Rohit, G.; Banerjee, U. C.; Chakraborti, A. K. 2-(2-Arylphenyl)-benzoxazole As a Novel Anti-Inflammatory Scaffold: Synthesis and Biological Evaluation. *ACS Med. Chem. Lett.* **2014**, *5*, 512−516.

(35) Shah, P.; Dhameliva, T. M.; Bansal, R.; Nautival, M.; Kommi, D. N.; Jadhavar, P. S.; Sridevi, J. P.; Yogeeswari, P.; Sriram, D.; Charkraborti, A. K. 2-*N*-Arylalkylbenzo-[*d*]thiazole-2-carboxamides as anti-mycobacterial agents: design, new methods of synthesis and biological evaluation. *Med. Chem. Commun.* **2014**, *5*, 1489−1495.

(36) Dhameliva, T. M.; Tiwari, R.; Banerjee, A.; Pancholia, S.; Sriram, D.; Panda, D.; Chakraborti, A. K. 4-Benzo[*d*]thiazole-2-carbanilides as new anti-TB chemotypes: Design, synthesis, biological

https://doi.org/10.1021/acsomega.2c06954
ACS Omega 2023, 8, 5571−5592

evaluation, and structure-activity relationship. *Eur. J. Med. Chem.* **2018**, *155*, 364−380.
(37) Bhagat, S.; Supriya, M.; Pathak, S.; Sriram, D.; Chakraborti, A. K. α-Sulfonamidophosphonates as new anti-mycobacterial chemotypes: Design, development of synthetic methodology, and biological evaluation. *Bioorg. Chem.* **2019**, *82*, 246−252.
(38) Jadhavara, P. S.; Patela, K. I.; Dhameliyaa, T. M.; Sahaa, M.; Vajaa, M. D.; Krishnab, V. S.; Sriramb, D.; Chakrabortia, A. K. Benzimidazoquinazolines as new potent anti-TB chemotypes: Design, synthesis, and biological evaluation. *Bioorg. Chem.* **2020**, *99*, No. 103774.
(39) Kerru, N.; Singh, P.; Koorbanally, N.; Jaj, R.; Kumar, V. Recent advances (2015−2016) in anticancer hybrids. *Eur. J. Med. Chem.* **2015**, *142*, 179−212.
(40) Kryshchyshyn, A.; Roman, O.; Lozynskyi, A.; Lesyk, R. Thiopyrano[2,3-*d*]thiazoles as new efficient scaffolds in medicinal chemistry. *Sci. Pharm.* **2018**, *86*, 26.
(41) Ardiansah, B. Recent reports on pyrazole-based bioactive compounds as candidate for anticancer agents. *Asian J. Pharm. Clin. Res.* **2017**, *12*, 45.
(42) Kumar, R. S.; Arif, A. I.; Ahmed, A.; Idhayadhulla, A. Antiinflammatory and antimicrobial activities of novel pyrazole analogues. *Saudi J. Biol. Sci.* **2016**, *23*, 614.
(43) Bennani, F. E.; Doudach, L.; Cherrah, Y.; Ramli, Y.; Karrouch, K.; Amsar, M.; Faouz, M. E. Overview of recent developments of pyrazole derivatives as an anticancer agent in different cell line. *Bioorg. Chem.* **2020**, *97*, No. 103470.
(44) Kuthyala, S.; Sheikh, S.; Prabhu, A.; Rekha, P. D.; Karikannar, N. G.; Shankar, M. K. Synthesis, Characterization, and Anticancer Studies of Some Pyrazole-Based Hybrid Heteroatomics. *ChemistrySelect* **2020**, *5*, 10827−10834.
(45) Maciejewska, N.; Olszewski, M.; Jurasz, J.; Serocki, M.; Dzierzynska, M.; Cekala, K.; ieczerzak, E.; Baginski, M. Novel chalcone-derived pyrazoles as potential therapeutic agents for the treatment of non-small cell lung cancer. *Sci. Rep.* **2021**, *12*, 3703.
(46) Ozdemir, A.; Altintop, M. D.; Kaplancikli, Z. A.; Can, O. D.; Ozkay, U. D.; Zitouni, G. T. Synthesis and evalution of new 1,5-diaryl-3-[4(methyl-sulfonyl)phenyl]-4,5-dihydro-1*H*-pyrazole derivatives as potential antidepressant agents. *Molecules* **2015**, *20*, 2668−2684.
(47) Metwally, N. H.; Badawy, M. A.; Okpy, D. S. Synthesis and anticancer activity of some new thiopyrano[2,3-*d*]thiazoles incorporating pyrazole moiety. *Chem. Pharm. Bull.* **2015**, *63*, 495−503.
(48) Metwally, N. H.; Abdelrazek, F. M.; Eldaly, S. M. Synthesis and anticancer activity of some new heterocyclic compounds based on 1-cyanoacetyl-3,5-dimethylpyrazole. *Res. Chem. Intermed.* **2016**, *42*, 1071−1089.
(49) Metwally, N. H.; Abdelrazek, F. M.; Eldaly, S. M. Synthesis, molecular docking, and biological evaluation of some novel bis-heterocyclic compounds based *N*,*N*′-([1,1′-biphenyl]-4,4′-diyl)bis(2-cyanoacetamide) as potential anticancer agents. *J. Heterocycl. Chem.* **2018**, *55*, 2668−2682.
(50) Metwally, N. H.; Deeb, E. A. Synthesis, anticancer assessment on human breast, liver and colon carcinoma cell lines and molecular modeling study using novel pyrazolo[4,3-*c*]pyridine derivatives. *Bioorg. Chem.* **2018**, *77*, 203−214.
(51) Metwally, N. H.; Badawy, M. A.; Okpy, S. M. Green synthesis of some new thiopyrano[2,3-*d*][thiazolo][1,3]thiazoles using lemon juice and their antibacterial activity. *Synth. Commun.* **2018**, *48*, 2496−2509.
(52) Metwally, N. H.; Mohamed, M. S.; Ragb, E. A. Design, synthesis, anticancer evaluation, mol-ecular docking and cell cycle analysis of 3-methyl-4,7-dihydropyrazolo[1,5-*a*]pyrimidine derivatives as potent histone lysine demethylases (KDM) inhibitors and apoptosis inducers. *Bioorg. Chem.* **2019**, *88*, No. 102929.
(53) Metwally, N. H.; Saad, G. R.; Abdwahab, E. A. Grafting of multiwalled carbon nanotubes with pyrazole derivatives: Characterization, antimicrobial activity and molecular docking study. *Int. J. Nanomed.* **2019**, *20*, 6645−6659.
(54) Metwally, N. H.; Mohamed, M. S. New imidazolone derivatives comprising a benzoate or sulfonamide moiety as anti-inflammatory and antibacterial inhibitors: Design, synthesis, selective COX-2, DHFR and molecular-modeling study. *Bioorg. Chem.* **2020**, *99*, No. 103438.
(55) Metwally, N. H.; Abdallah, S. O.; Mohsen, M. M. A. Design, green one-pot synthesis and molecular docking study of novel *N*,*N*-bis(cyanoacetyl) hydrazines and bis-coumarins as effective inhibitors of DNA gyrase and topoisomerase IV. *Bioorg. Chem.* **2020**, *97*, No. 103672.
(56) Metwally, N. H.; Mohamed, M. S.; Deeb, E. A. Synthesis, anticancer evaluation, CDK2 inhibition, and apoptotic activity assessment with molecular docking modeling of new class of pyrazolo[1,5-*a*]pyrimidines. *Res. Chem. Intermed.* **2021**, *47*, 5027−5060.
(57) Metwally, N. H.; Abd-Elmoety, A. S. Novel fluorinated pyrazolo[1,5-*a*]pyrimidines: In a way from synthesis and docking studies to biological evaluation. *J. Mol. Struct.* **2022**, *1257*, No. 132590.
(58) Metwally, N. H.; Badawy, M. A.; Okpy, D. S. Synthesis, biological evaluation of novel thiopyrano[2,3-*d*]thiazoles incorporating arylsulfonate moiety as potential inhibitors of tubulin polymerization, and molecular modeling studies. *J. Mol. Struct.* **2022**, *1258*, 132848.
(59) Mase, N.; Horibe, T. Organocatalytic Knoevenagel condensations by means of carbamic acid ammonium salts. *Org. Lett.* **2013**, *15*, 1854−1857.
(60) Kryshchyshyn, A.; Roman, O.; Lozynskyi, A.; Lesyk, R. Thiopyrano[2,3-*d*]thiazoles as new efficient scaffolds in medicinal chemistry. *Sci. Pharm.* **2018**, *86*, 26.
(61) Lozynskyi, A.; Matiychuk, V.; Karpenko, O.; Gzella, A. K.; Lesyk, R. Tandem hetero-Diels−Alder-hemiacetal reaction in the synthesis of new chromeno[4′,3′:4,5] thiopyrano[2,3-*d*]thiazoles. *Heterocycl. Commun.* **2017**, *23*, 1−5.
(62) Li, P.; Zhou, L.; Zhao, T.; Liu, X.; Zhang, P.; Liu, Y.; Zheng, X.; Li, O. Caspase-9: structure, mechanisms and clinical application. *Oncotarget.* **2017**, *8*, 23996−24008.
(63) Komaritsa, I. D.; Baranov, S. N.; Grischuk, A. P. 4-Thiazolidines, derivatives and analogs. *Chem. Heterocycl. Compd.* **1967**, *3*, 533−534.
(64) Kiro, M. A.; Abdel-Rahman, M. O.; Gadalla, K. Z. The vilsmeier-haack reaction-III-cyclization of hydrazones to pyrazoles. *Tetrahedron Lett.* **1696**, *2*, 109−110.
(65) Cava, M. P.; Deana, A. A.; Muth, K.; Mitchell, M. *N*-Phenylmaleimides. *Org. Synth.* **1961**, *41*, 93−95.
(66) Mosmann, T. Rapid colorimetric assay for cellular growth and survival: application to proliferation and cytotoxicity assays. *J. Immunol. Methods* **1983**, *65*, 55−63.
(67) Denizot, F.; Lang, R. Rapid colorimetric assay for cell growth and survival. *J. Immunol. Methods* **1986**, *89*, 271−277.
(68) Ozdemir, H. O.; Cetinkaya, R. Effects of glycation on erythrocyteanhydrase-I and II patients with diabetes mellitus. *Turk. J. Med. Sci.* **2000**, *30*, 135−141.
(69) Hilvo, M.; Baranauskiene, L.; Salzano, A. M.; Scaloni, A.; Matulis, D.; Innocenti, A.; Scozzafava, A.; Kulomaa, S. M.; Nordlund, H. R.; Supuran, C. T.; Parkkila, S. Biochemical characterization of CA IX, one of the most active carbonic anhydrase isozymes. *J. Biol. Chem.* **2008**, *283*, 27799−27809.
(70) Burnett, W. N. Western blotting: electrophoretic transfer of protein from sodium dodecyl sulfate-polyacrylamide gels to unmodified nitrocellulose and radiographic detection with antibody and radioiodinated protein A. *Anal. Biochem.* **1981**, *112*, 195−203.
(71) Sambrook, J.; Fritsch, E. F.; Maniatis, T. *Molecular cloning: A laboratory manual*; Cold Spring Harbor Laboratory: New York. 1989.
(72) C. C. Group, *Chemical Computing Group and Molecular Networks Announce the Integration of CORINA into MOE*; C. C. Group 2007.
(73) Chrysanthopoulos, P. K.; Mujumdar, P.; Woods, L. A.; Dolezal, O.; Ren, B.; Peat, T. S.; Poulsen, S. A. Identification of a New Zinc

https://doi.org/10.1021/acsomega.2c06954
ACS Omega 2023, 8, 5571−5592

Binding Chemotype by Fragment Screening. *J. Med. Chem.* **2017**, *60*, 7333−7349.

https://doi.org/10.1021/acsomega.2c06954
ACS Omega 2023, 8, 5571−5592